HHS Public Access

Author manuscript

*Neuron*. Author manuscript; available in PMC 2018 September 27.

Published in final edited form as:

*Neuron*. 2017 September 27; 96(1): 115–129.e5. doi:10.1016/j.neuron.2017.09.003.

# Apolipoprotein E4 impairs neuronal insulin signaling by trapping insulin receptor in the endosomes

**Na Zhao**[1,4], **Chia-Chen Liu**[1,4,*], **Alexandra J. Van Ingelgom**[1], **Yuka A. Martens**[1], **Cynthia Linares**[1], **Joshua A. Knight**[1], **Meghan M. Painter**[1], **Patrick M. Sullivan**[2], and **Guojun Bu**[1,3,5,*]

[1]Department of Neuroscience, Mayo Clinic, Jacksonville, FL, 32224, USA

[2]Departments of Medicine, Duke University School of Medicine; GRECC, Durham Veterans Affairs Medical Center, Durham, NC, 27705, USA

[3]Fujian Provincial Key Laboratory of Neurodegenerative Disease and Aging Research, Institute of Neuroscience, College of Medicine, Xiamen University, Xiamen, Fujian, 361005, China

## SUMMARY

Diabetes and impaired brain insulin signaling are linked to the pathogenesis of Alzheimer's disease (AD). The association between diabetes and AD-associated amyloid pathology is stronger among carriers of the apolipoprotein E (*APOE*) ε4 gene allele, the strongest genetic risk factor for late-onset AD. Here we report that apoE4 impairs neuronal insulin signaling in human apoE-targeted replacement (TR) mice in an age-dependent manner. High fat diet (HFD) accelerates these effects in apoE4-TR mice at middle age. In primary neurons, apoE4 interacts with insulin receptor and impairs its trafficking by trapping it in the endosomes, leading to impaired insulin signaling and insulin-stimulated mitochondrial respiration and glycolysis. In aging brains, the increased apoE4 aggregation and compromised endosomal function further exacerbate the inhibitory effects of apoE4 on insulin signaling and related functions. Together, our study provides novel mechanistic insights into the pathogenic mechanisms of apoE4 and insulin resistance in AD.

## In Brief

Zhao et al. demonstrates that aging and peripheral insulin resistance induces impairment of cerebral insulin signaling in human apoE4-targeted replacement mice. ApoE4 interferes with insulin receptor signaling by blocking its interaction with insulin and trapping the receptor in the endosomes.

[*]Correspondence should be addressed to Guojun Bu (bu.guojun@mayo.edu) or Chia-Chen Liu (liu.chiachen@mayo.edu).

[4]These authors contributed equally to this work.

[5]Lead contact.

**AUTHOR CONTRIBUTIONS**

NZ, C-CL and GB designed the experiments and wrote the paper. NZ, C-CL and AVI executed the experiments, analyzed the data and completed the statistical analysis. YAM prepared the truncated apoE. CL and JAK contributed to the animal maintenance and tissue preparation. MMP provided advice on cellular trafficking studies and edited the manuscript. PMS developed and contributed the apoE-TR mice. All authors read and commented on the manuscript.

## INTRODUCTION

Alzheimer's disease (AD) is an age-related metabolic neurodegenerative disease (Jack et al., 2010). Diabetes and impaired insulin signaling in the brain are linked to the pathogenesis of AD (Biessels et al., 2006; Bomfim et al., 2012; Talbot et al., 2012). Levels of insulin, insulin receptor (IR), and insulin signaling are lower in AD brains and epidemiological studies have confirmed that diabetic patients are at higher risk for AD (Craft et al., 2013; Hoyer, 2004; Steen et al., 2005). Furthermore, peripheral insulin resistance, a prevalent and increasingly common condition in developed countries, is associated with significantly lower regional cerebral glucose metabolism, which in turn predicts worse memory performance (Willette et al., 2015). Supporting these, recent Phase II clinical trials with insulin nasal spray in AD patients have yielded positive results in preventing cognitive decline and this has led to a new national plan for Phase II/III trials (Claxton et al., 2015; Claxton et al., 2013). Thus, there is an urgent need to understand the function and regulation of brain insulin signaling in preclinical models.

The ε4 allele of the apolipoprotein E (*APOE*) gene is the strongest genetic risk factor for AD compared to the common ε3 allele and the protective ε2 allele (Bu, 2009; Liu et al., 2013; Zhao et al., 2017). Although apoE4 has been shown to impair amyloid-β (Aβ) clearance and promotes Aβ aggregation leading to enhanced amyloid pathology, increasing evidence suggests that apoE isoforms differentially regulate brain insulin signaling and glucose metabolism (Peila et al., 2002; Reiman et al., 1996; Small et al., 1995). FDG-PET studies showed that *APOE4* carriers, either as healthy adults or with dementia, have lower cerebral glucose metabolism (Reiman et al., 1996; Reiman et al., 2005). Recent clinical trials have also revealed that the beneficial effects of intranasal insulin treatment on cognitive improvement in AD patients are modulated by *APOE* genotype status (Claxton et al., 2015; Claxton et al., 2013; Reger et al., 2006). The important role of apoE-mediated modulation of insulin signaling and glucose metabolism is further supported by our recent observation that conditional deletion of a major apoE receptor, LRP1, in mouse forebrain neurons leads to impaired brain insulin signaling and a reduced capacity to metabolize glucose (Liu et al., 2015). Thus, it is crucial to define the molecular and cellular mechanisms by which apoE isoforms differentially influence brain insulin signaling.

Herein, we show that apoE4-targeted replacement (TR) mice, in which the endogenous murine *Apoe* is replaced by human apoE4, exhibit an impaired insulin signaling and insulin resistance in the brain in an age-dependent manner. High-fat-diet (HFD)-induced peripheral insulin resistance further exacerbates the impairment of insulin signaling and insulin response in apoE4-TR mice. More importantly, we demonstrate that apoE4 interacts with IR and impairs its trafficking and related signaling by trapping it in the endosomes. Finally, we found that the increased apoE4 aggregation and compromised endosomal function exacerbate the inhibitory effects of apoE4 on insulin signaling and related functions with aging. Together, our study reveals novel mechanisms by which apoE4 and insulin resistance contribute to AD, providing biological insights into apoE-targeted therapies to improve cerebral insulin signaling to treat AD.

# RESULTS

## Age-dependent Impairment of Cerebral Basal Insulin Signaling in ApoE4-TR Mice

Impaired insulin signaling in the central nervous system (CNS) has been linked to the pathogenesis of AD (Craft and Watson, 2004). Given that the effects on cognition upon intranasal insulin treatment in adults with dementia are influenced by *APOE* genotype (Reger et al., 2006), we reasoned that insulin signaling in the brain may be affected by different apoE isoforms. In the canonical insulin signaling pathway, insulin binds to its cognate receptor on the plasma membrane which induces signal transduction including phosphorylation of Akt. In turn, activated Akt phosphorylates and inhibits GSK3β which results in dephosphorylation of GSK3β substrates (Cohen and Frame, 2001). Therefore, we examined the major downstream molecules involved in insulin signaling in brain homogenates of apoE3- and apoE4-TR mice at 3, 12 and 22 months of age, representing young, middle and old ages, respectively. Intriguingly, we found that the levels of these key insulin-related signaling molecules including phosphorylated-Akt (p-Akt) and phosphorylated-GSK3β (p-GSK3β) were significantly decreased in both cortex (Figures 1A–C) and hippocampus (Figures 1D–F) of apoE4-TR mice at 22 months of age. However, there were no significant differences in the amount of p-Akt and p-GSK3β in the cortical fractions of apoE3- and apoE4-TR mice at 3 or 12 months of age (Figures 1G–L). To further confirm the specific changes of insulin signaling pathway in these mice, we also examined the levels of phosphorylated-IR (p-IR) which is the upstream molecular of p-Akt. Significantly decreased ratio of p-IR to total IR was detected in the cortex of apoE4-TR mice at 22 months of age compared with apoE3-TR mice (Figure S1A), with no difference between apoE3-TR and apoE4-TR mice at 3 months of age (Figure S1B), indicating that basal insulin signaling is impaired in apoE4-TR mice in an age-dependent manner.

To further examine whether apoE4 affects insulin signaling pathway in the peripheral tissues of aged apoE4-TR mice, we examined the levels of p-Akt and p-GSK3βin the skeletal muscle and liver, two critical sites contributing to peripheral insulin signaling (DeFronzo and Tripathy, 2009; Michael et al., 2000). There were no significant differences in the amount of p-Akt and p-GSK3β in the skeletal muscle (Figures S2A–C) and liver (Figures S2D–F) of apoE3-TR and apoE4-TR mice at 22 months of age, indicating that the basal peripheral insulin signaling remains intact in aged apoE4-TR mice.

## High-Fat Diet (HFD)-induced Peripheral Insulin Resistance Accelerates Age-dependent Impairment of Basal Insulin Signaling in the Brain of ApoE4-TR Mice

Type 2 diabetes characterized by peripheral insulin resistance, impaired insulin signaling and glucose intolerance are associated with cognitive impairment (Ott et al., 1999). To examine the synergistic interaction between *APOE4* and type 2 diabetes in brain insulin signaling, we investigated whether peripheral insulin resistance impairs cerebral insulin signaling in an apoE isoform-dependent manner using a HFD-induced insulin resistance mouse model. The 8-month-old apoE3- and apoE4-TR mice were fed with HFD (60% fat) or normal fat (5.8%) diet (NFD) for 4 months. The fasting glucose levels of HFD-fed mice (apoE3-TR mice: 171.54 ± 10.08 mg/dL; apoE4-TR mice: 166.71 ± 14.75 mg/dL) were significantly higher than NFD-fed mice (apoE3-TR mice: 119.25 ± 7.63 mg/dL; apoE4-TR mice: 123.42 ± 8.08

mg/dL) supporting a peripheral insulin-resistance phenotype after HFD treatment (Winzell and Ahren, 2004). Intriguingly, apoE4-TR mice fed with HFD exhibited a significant decrease in the activation of downstream insulin signaling, indicated by the reduced ratios of p-Akt/Akt and p-GSK3β/GSK3β in the cortex (Figure 2A) and hippocampus (Figure 2B) compared with HFD-fed apoE3-TR mice at 12 months of age. These apoE isoform-dependent effects were not observed in mice fed with NFD. These results demonstrate that HFD-induced peripheral insulin resistance and apoE4 synergistically reduce cerebral insulin signaling.

## ApoE4 Reduces Tissue Sensitivity to Insulin Stimulation

Cerebral insulin resistance, indicated by reduced cellular responsiveness to insulin, is a common pathological feature of AD (Sims-Robinson et al., 2010; Talbot et al., 2012). We thus sought to investigate whether apoE4 affects the insulin sensitivity in the brain. Insulin was delivered to the left hippocampus of aged apoE-TR mice or HFD-treated apoE-TR mice via reverse microdialysis and insulin signaling was evaluated in both ipsilateral and contralateral sides of insulin delivery. We found that the increase of insulin-induced signaling in the hippocampus was significantly lower in apoE4-TR mice compared with apoE3-TR mice both under aged condition (Figure 3A) and HFD treatment (Figure 3B), suggesting that aged apoE4-TR mice develop cerebral insulin resistance that can be further accelerated by HFD-induced peripheral insulin resistance conditions.

IR has been shown to be more concentrated in neurons relative to glial cells in the brain and its distribution is particularly high in post-synaptic density (Unger et al., 1991), suggesting a critical role of insulin signaling in neurons. Thus, we first tested how apoE isoforms affect the response of insulin in neurons. *Apoe*$^{-/-}$ primary neurons were treated with recombinant apoE3 or apoE4, followed by insulin stimulation. Similar to the *in vivo* results, apoE4 treatment led to reduced insulin signaling in primary neurons (Figure 3C), suggesting that apoE4 suppresses the action of insulin in neurons.

To examine the effects of apoE on the peripheral insulin-stimulated responses, we detected the activation of insulin signaling in the skeletal muscle of aged apoE-TR mice after injection of insulin into inferior vena cava. We found that the increase of insulin signaling in the skeletal muscle was significantly lower in aged apoE4-TR mice compared with that in apoE3-TR mice (Figure S3A). ApoE4 also inhibited the activation of insulin signaling in HuH7 hepatoma cells (Figure S3B). These results suggest that apoE4 may reduce the peripheral insulin sensitivity upon insulin stimulation.

## ApoE4 Inhibits Insulin-induced Effects on Mitochondrial Respiration and Glycolysis in Primary Neurons

Recent evidence indicates that insulin resistance and mitochondrial dysfunction are common pathological features connecting type 2 diabetes to AD (De Felice and Ferreira, 2014). It has been reported that insulin could regulate both mitochondrial respiration and glycolysis, the two major pathways of energy metabolism (Beitner and Kalant, 1971; Garcia-Caceres et al., 2016; Nisr and Affourtit, 2014). To further investigate how apoE4 alters the function of insulin signaling on energy metabolism, we evaluated intracellular mitochondrial respiration

and glycolysis simultaneously by Seahorse XF96 Extracellular Flux analyzer, a sensitive, high-throughput instrument (Zhang et al., 2012). Using this technology, we were able to quantitatively compare intracellular glucose-mediated energy metabolism in neurons treated with different apoE isoforms. The *Apoe*$^{-/-}$ neurons were treated with vehicle or recombinant apoE3 or apoE4 protein overnight in insulin-free media followed by 30 minitues insulin treatment. To test mitochondrial respiration, bioenergetic profiles were created in which changes in oxygen consumption rate (OCR) were assessed over time after sequential injections of different inhibitory compounds for the critical enzymes in the electron transport chain of the mitochondria (Figures 4A–C). Based on these profiles, basal respiration and maximal respiration were calculated. To measure glycolysis, the extracellular acidification rate (ECAR), produced indirectly following glucose to lactate conversion independent of oxygen, was assessed over time and these profiles were used to calculate glycolysis rate and glycolytic capacity (Figures 4D–F). We observed that insulin significantly increased basal and maximal mitochondrial respiration (Figure 4A), glycolysis rate and glycolytic capacity (Figure 4D) in *Apoe*$^{-/-}$ neurons. ApoE3 treatment neither affected insulin-induced mitochondrial respiration (Figure 4B) nor glycolysis (Figure 4E). Interestingly, apoE4 treatment significantly inhibited insulin's ability to increase neuronal mitochondrial respiration (Figure 4C) and glycolysis (Figure 4F).

To further confirm these results, we treated *Apoe*$^{-/-}$ neurons with astrocyte-secreted apoE3 or apoE4 lipoprotein particles that are lipidated and more closely mimic the biochemical properties of apoE *in vivo*. Similarly, lipidated apoE4 but not apoE3 particles inhibited insulin-induced effects on mitochondrial respiration and glycolysis (Figures S4A–F). These results indicate that apoE4, but not apoE3, suppresses insulin-stimulated mitochondrial respiration and glycolysis in neurons.

## ApoE4 Interacts with Insulin Receptor and Impairs its Trafficking

Internalization of IR has been shown to play a critical role in the signaling events (Di Guglielmo et al., 1998; Kublaoui et al., 1995). Insulin signaling is initiated through the binding of insulin to the cell surface IR, a disulfide-linked heterotetramer consisting of two homologous α and β subunits. Upon insulin binding to the extracellular α subunit of IR, a conformational change of IR leads to β subunit autophosphorylation, which triggers the rapid endocytosis of the insulin-IR complex with concomitant downstream signaling activation (Carpentier et al., 1978; Gorden et al., 1978). Once IR is sequestered from insulin in the endosomal compartment, the majority of receptor is recycled back to the plasma membrane, presumably for another round of ligand binding and internalization, while a small amount of the receptor is destined to lysosome for degradation (Baldwin et al., 1980; Trischitta et al., 1989). Thus, to investigate how apoE4 impairs insulin signaling, we first investigated whether apoE4 could disrupt insulin and IR interaction by binding to either insulin or IR. Using a solid-phase binding assay in which recombinant insulin or IR was incubated with immobilized apoE3 or apoE4, we did not detect a specific binding between apoE and insulin (data not shown). Conversely, we found that both recombinant apoE3 and apoE4 specifically bound to IR with apoE4 having higher binding affinity than apoE3 (Figure 5A). Furthermore, we examined the interaction of IR with lipidated apoE purified from the conditioned medium of astrocytes, a physiologically more relevant source of brain

apoE. Importantly, the binding affinities of astrocyte-secreted apoE3 and apoE4 lipoprotein particles for IR were ~10 times higher than their corresponding recombinant apoE (Figure 5B). Similar to recombinant apoE, we found that apoE4 lipoprotein particles bind to IR more strongly than apoE3 lipoprotein particles (Figure 5B). No specific binding was detected between IR and apolipoprotein J (apoJ, also known as clusterin) (Figure S5), another important lipoprotein in the brain that has been implicated in AD pathogenesis (Calero et al., 2000). These findings support the binding specificity between apoE and IR. In addition, we further verified the binding of apoE to IR using a solution binding assay followed by co-immunoprecipitation. Recombinant apoE and IR were co-incubated for one hour at 37°C, and the apoE was pulled down by an apoE-specific antibody. We found that more IR was co-immunoprecipitated with apoE4 than with apoE3 (Figure 5C). To further identify the interacting domain of apoE, we performed solid-phase binding assays to assess the binding of IR with full-length (FL) apoE (aa1-299) or C-terminal truncated apoE (aa1-186) (Figures 5D, E). Interestingly, the binding ability of truncated apoE to IR was significantly decreased, with 50% reduction in truncated apoE3 (Figure 5D) and 30% reduction in truncated apoE4 (Figure 5E) compared to the FL apoE, indicating the involvement of C-terminal domain of apoE in IR binding. Taken together, these data demonstrated that apoE binds to IR in an isoform-dependent manner with apoE4 showing higher binding affinity than apoE3.

To further confirm the interaction between apoE and IR *in vivo*, we immunoprecipitated apoE from the brain lysates of young (3 month) or old (22 month) apoE-TR mice. Interestingly, IR was co-immunoprecipitated with apoE in old apoE4-TR mice but not in apoE3-TR mice or in young apoE4-TR mice under these experimental conditions (Figure S6A). We also performed the assay in a reciprocal fashion in which apoE was co-immunoprecipitated with IR exclusively in 22-month-old apoE4-TR mice (Figure S6B), suggesting an increased binding between apoE4 and IR with aging.

To examine whether apoE4 interferes with the interaction between insulin and IR, we determined the kinetics of insulin-IR binding using solid-phase binding assay. Based on this binding kinetics, we chose appropriate insulin and IR concentrations for the apoE competition experiments. When apoE was co-incubated with insulin and IR, we found that apoE4 (16 μg/ml) reduced insulin-IR binding by nearly 50%, which is significantly higher than apoE3 treatment (25%) (Figure 5F). These results indicate that apoE interferes with insulin-IR interaction in an isoform-dependent manner with apoE4 exhibiting greater detrimental effects.

Since insulin binding to IR triggers its translocation from the plasma membrane to the endosomal compartment, an event that is important for the full activation of signaling cascade (Di Guglielmo et al., 1998; Kublaoui et al., 1995), we next investigated whether apoE isoforms differentially affect IR internalization. $Apoe^{-/-}$ neurons were treated with different apoE isoforms and the amount of cell surface IR was evaluated by cell surface biotinylation assay. In the absence of insulin stimulation, we found that apoE4 but not apoE3 significantly reduced the amount of cell surface IR (Figures 5G, H). Importantly, ~50% of the total IR was internalized in response to insulin in apoE3-treated cells, whereas only ~20% of IR was internalized in apoE4-treated cells upon insulin stimulation (Figure 5I).

These results were consistent with our observations that apoE4 suppressed the activation of insulin signaling compared to apoE3 (Figures 5G, J, K and 3C), likely by blocking the insulin-IR interaction and thus suppressing IR internalization and signaling activation. Moreover, as apoE4 downregulates cell surface IR even in the absence of insulin, it is possible that in the presence of apoE4 less amount of IR is available on the surface for the action of insulin.

Previous study reported that the recycling of apoE4 is impaired in primary neurons in which more apoE4 is retained within intracellular compartments compared with apoE3 (Chen et al., 2010). Thus, we hypothesized that decreased cell surface IR following apoE4 treatment resulted from an impairment of apoE4-related trafficking. To test this, we expressed human IR tagged with GFP in SH-SY5Y neuronal cells and tracked IR-GFP localization following treatment with apoE isoforms in the presence or absence of insulin stimulation. In the absence of insulin, the majority of the IR-GFP was localized to the cell membrane with only 15% of the receptor localized intracellularly in apoE3-treated cells (Figures 6A–C). Interestingly, nearly 40% of IR-GFP was localized in the intracellular compartment in apoE4-treated cells (Figures 6A–C), consistent with our observation in which apoE4 reduced cell surface IR (Figures 5G–I). Importantly, insulin stimulation increased the percentage of intracellular IR-GFP in apoE3-treated, but not in apoE4-treated, cells (Figures 6A–C).

To investigate the intracellular trafficking and distribution of IR after incubation with apoE and/or insulin, IR-GFP-expressing cells were labeled with Alexa Flour 568-conjugated transferrin (Tf), a marker of the early endosome and recycling endosome. In the absence of insulin, we found that nearly 20% of IR-GFP co-localized with transferrin in the endosomal compartment in apoE4-treated cells whereas less co-localization was observed in apoE3-treated cells (Figures 6A and 6D). Insulin induced IR internalization which increased the co-localization of IR-GFP with transferrin in apoE3-treated cells, but not in apoE4-treated cells (Figures 6A and 6D). No differences were observed for the co-localization of IR-GFP with Lysotracker, a lysosomal marker, between apoE3- and apoE4-treated cells, with or without insulin (Figures 6B and 6E). These results suggest that the slower recycling of apoE4 might trap IR in the endosomal compartment; thereby impairing its ability to bind insulin and trigger IR signaling at the cell surface.

We next investigated whether apoE4 affects the trafficking of other membrane receptors in neurons, including the low-density lipoprotein receptor-related protein 1 (LRP1), N-methyl-D- aspartate receptor (NMDAR) and α-amino-3-hydroxy-5-methyl-4- isoxazolepropionic acid receptor (AMPAR), as well as a plasma membrane marker Na-K-ATPase. *Apoe*$^{-/-}$ neurons were treated with different apoE isoforms and the amount of cell surface IR, LRP1, NMDAR, AMPAR, and Na-K-ATPase were evaluated by cell surface biotinylation assay. As expected, cell surface IR was decreased after treatment with apoE4 compared with apoE3 (Figures S7A, B) without affecting the total IR (Figures S7A, G). No significant differences were found in the levels of cell surface and total LRP1, NMDAR, AMPAR, and Na-K-ATPase after apoE3 and apoE4 treatments (Figures S7A, C–F, H–K). These results indicate that apoE4 specifically suppresses cell surface IR in neurons.

To directly test how apoE isoforms differentially affect IR trafficking, we evaluated the internalization and recycling of IR using cell-surface biotinylation techniques in cultured *Apoe*$^{-/-}$ cortical neurons. The internalization of IR reached plateau at 30 minutes after treatment with either apoE3 or apoE4 (Figure S8A). After 60 minutes treatment with apoE3, the amount of internalized (biotinylated) IR was reduced, reflecting a membrane recycling of IR and subsequent biotin cleavage. Interestingly, apoE4-treated cells exhibited significantly more intracellular IR compared to those treated with apoE3 at 60 minutes, suggesting a delayed recycling of IR in the presence of apoE4 (Figure S8A). A recycling assay was then performed to further confirm this finding. Cells were treated with apoE3 or apoE4 for 30 minutes to allow the maximal internalization of biotinylated IR. After removal of apoE, the biotinylated IR that recycled back to cell surface was removed by glutathione cleavage. Thus, the reduction of intracellular (biotinylated) IR over time represents the recycling of this receptor. Intriguingly, significantly higher amount of intracellular IR was detected in apoE4-treated cells compared with cells treated with apoE3 at 30 minutes and 60 minutes, indicating that apoE4 impaired IR recycling (Figure S8B). To further test how apoE isoforms differentially affect insulin-induced IR trafficking, we monitored IR internalization after insulin treatment in the absence or presence of apoE. Insulin induced rapid endocytosis of IR with the plateau appeared at 5 minutes and then steadily declined, reflecting membrane recycling of IR and subsequent biotin cleavage (Figure S9). In the presence of apoE3, the plateau of the curve shifted to 15 minutes and then started to decline (Figure S9). However, in the presence of apoE4, the internalization of IR did not approach plateau until 30 minutes and without obvious decline over time (Figure S9), indicating that apoE4 inhibited insulin-induced IR trafficking.

## ApoE4 Accelerates the Aggregation of IR with Aging

Aggregation of certain cellular proteins is a common feature of aging in particular under aging-related neurodegenerative conditions (David et al., 2010; Lindner and Demarez, 2009). We speculate that apoE4 may be prone to aggregation during aging which can in turns impair the functions of IR and insulin signaling in an age-dependent manner. To examine the aggregation status of apoE isoforms and IR in the brains, the cortex of young (3 months of age) and aged (22 months of age) apoE-TR mice was sequentially extracted with RIPA buffer (detergent-soluble fraction), and guanidine (GND, detergent-insoluble fraction). The levels of soluble apoE and IR in RIPA fractions were detected by Western blotting and ELISA; the insoluble apoE and IR in GND fractions, which contain the aggregated proteins, were detected by ELISA. The amounts of soluble apoE did not significantly differ between young and old mice regardless of *APOE* genotypes (Figures 7A, B, D). Intriguingly, the level of insoluble apoE was significantly increased in aged apoE4-TR mice compared with that in young mice (Figure 7E), leading to an increased insoluble to soluble ratio of apoE with aging (Figure 7F). To a lesser extent, there was a trend of an increased insoluble to soluble apoE ratio with aging in apoE3-TR mice (Figures 7E, F). The increase of insoluble apoE4 in aged brain suggests that apoE4 might be more prone to aggregation with aging compared to apoE3. Moreover, the level of detergent-soluble IR was significantly decreased with aging in apoE4-TR mice, but not in apoE3-TR mice (Figures 7A, G). Though the insoluble IR was increased in aged mice with either *APOE* genotype (Figure 7H), the ratio of insoluble to soluble IR was found to be significantly increased only in aged apoE4-TR

mice (Figure 7I). Taken together, these results suggest that apoE4 might be more likely to aggregate during aging, which accelerates IR aggregation and impaired functions.

### ApoE4 Induces Early Endosomal Abnormality with Aging

Endocytosis is crucial to various cellular functions, including inter-cellular communication, signal transduction, and metabolism; thus, even subtle abnormality in the endocytic compartments of cells in the brain may have a substantial impact on neuronal functions (Nixon, 2005). The enlargement of Rab5-positive endosomes has been shown to occur early and precede the onset of axonal dysfunction and AD pathogenesis (Ginsberg et al., 2010; Grbovic et al., 2003; Xu et al., 2016). Furthermore, it was shown that the presence of *APOE4* accentuates Rab5-positive endosomal enlargement at preclinical stages of AD (Cataldo et al., 2000). To test how apoE isoforms differently affect endocytic system with aging, we performed Rab5 staining with brain slices from apoE-TR mice at 3 months or 22 months of age. There was a significant up-regulation of Rab5 immunoreactivity in the cortex and amygdala regions of apoE4-TR mice at 22 months of age compared with that of apoE3-TR mice (Figures 8A–C), whereas no difference was found among 3-month-old apoE-TR mice (Figures S10A–C), suggesting an age-related endocytic dysfunction in apoE4-TR mice. Thus, the compromised endosomal function may exacerbate the inhibitory effects of apoE4 on insulin signaling and related functions with aging.

## DISCUSSION

Impaired insulin signaling has been demonstrated in both postmortem human AD brains and in mouse models of AD (Hoyer, 2004; Steen et al., 2005). Interestingly, in clinical trials the beneficial role of intranasal insulin delivery on improving cognition in AD patients is modulated by *APOE* genotype status (Claxton et al., 2015; Claxton et al., 2013; Reger et al., 2006). In this study, we found that apoE4 impairs cerebral insulin signaling in an age-dependent manner *in vivo*, consistent with a previous report (Ong et al., 2014). Additionally, HFD-induced peripheral insulin resistance and apoE4 synergistically impair cerebral insulin signaling. By delivering insulin into the mouse brain via the *in vivo* reverse microdialysis approach, or by administrating insulin into peripheral organ through the inferior vena cava injection, we found apoE4 reduces both the cerebral and peripheral responsiveness of insulin-induced signaling. Most importantly, we demonstrated that apoE4 impairs neuronal insulin signaling by binding to IR and trapping IR in the endosomes. Furthermore, we found that apoE4 accelerates IR aggregation and is associated with endocytic abnormality with aging. Our findings provide new insights into the molecular mechanisms responsible for the apoE isoform effects on cerebral insulin signaling, providing mechanistic insights for insulin-based AD prevention and therapy.

The action of insulin is initiated through binding to cell surface IR followed by internalization of the insulin-IR complex. Here, we demonstrated that apoE4 interacts with IR to block insulin binding to its cognate receptor (Figure S11). Using multiple approaches, we found that apoE4 binds to IR with higher affinity compared with apoE3; thus, apoE4 may block insulin-IR binding more efficiently. ApoE4 has been suggested to self-aggregate more easily than other apoE isoforms (Hatters et al., 2006), although there are some

discrepancies regarding to the dimerization of apoE (Aleshkov et al., 1997; Elliott et al., 2010; Martel et al., 1997; Weisgraber and Shinto, 1991). It is also possible that the aggregated apoE4 physically interferes with the interaction between IR and insulin. Consequently, apoE4 abrogates the action of insulin to induce IR internalization, which is critical for the maximal activation of insulin signaling. Furthermore, apoE4 exhibits a greater propensity to accumulate intracellularly following internalization due to impaired recycling (Heeren et al., 2004). The acidic environment in the early endosomal compartment has been proposed to enhance apoE4 self-aggregation (Morrow et al., 2002), which may further sequester interacting proteins including insulin receptor. Our current study showed that apoE4 suppresses cell surface IR by impairing IR trafficking, thereby more IR is retained in the early endosome together with apoE4. As a result, the downstream signaling and the effects of insulin-induced glycolysis and mitochondrial respiration are significantly suppressed by apoE4 (Figure S11). With aging, the increased apoE4 aggregation and compromised endosomal function exacerbate the inhibitory effects of apoE4 on insulin signaling and related functions (Figure S11). Chen and colleagues reported that apoE4 reduces surface level of Apoer2, a neuronal signaling receptor for Reelin and apoE, as well as glutamate receptors by sequestration them in intracellular compartments, thereby reducing synaptic activity (Chen et al., 2010; Lane-Donovan et al., 2014). These studies, including ours, suggest that apoE4 may suppress various signaling cascades by impairing the trafficking of cell surface receptors. The accumulation of proteins in the intracellular compartments might contribute to endocytic dysfunction during aging, which may further exacerbate the inhibitory effects of apoE4.

Since amyloid-β (Aβ) impairs insulin signaling both *in vivo* and *in vitro* (Craft et al., 2000; Craft et al., 2013; Craft and Watson, 2004; Hoyer, 2004; Steen et al., 2005), it will be important to examine whether Aβ further exacerbates apoE4-mediated deleterious effects on insulin signaling. It was reported that the disturbance of insulin signaling was worse in amyloid model mice expressing human apoE4 (ApoE4/APP) which correlates with poorer memory performance, compared with ApoE3/APP mice (Chan et al., 2015; Chan et al., 2016). However, it is still unclear whether Aβ and apoE4 play synergistic or competing roles in disrupting insulin signaling. It was shown that in the presence of Aβ, apoE4 bound more to Aβ whereas apoE3 bound more to IR (Chan et al., 2015). Our current findings demonstrate that apoE4 has higher binding affinity to IR in the absence of Aβ. Whether Aβ alters the binding status between IR and apoE isoforms requires further investigation. Furthermore, it was reported that IR is involved in the Aβ clearance, thus the dysfunction of IR impairs the intracellular clearance of oligomer Aβ in primary cultured neurons (Zhao et al., 2009). It will be interesting to test how apoE isoforms affect IR-regulated Aβ clearance.

Additionally, *APOE* genotype status appears to modulate cognitive responses to insulin and insulin-based AD therapies in several clinical trials. For example, AD patients who are *APOE4* non-carriers show memory facilitation after insulin infusion, whereas *APOE4* carriers are cognitively unaffected in response to insulin (Craft et al., 2000). Acute administration of short-acting intranasal insulin improves cognition in AD patients who are *APOE4* non-carriers, whereas no improvement is found in *APOE4* carriers treated with any of the doses (Reger et al., 2008). Interestingly, the long-acting intranasal insulin modulates cognition in AD patients with improvement for *APOE4* carriers and worsening for non-

carriers (Claxton et al., 2015). Our results that apoE4 impairs cerebral insulin signaling and induces insulin resistance might explain why acute intranasal insulin stimulation benefits *APOE4* non-carriers but not carriers. However, chronic insulin treatment might induce cerebral insulin resistance in *APOE4* non-carriers who have normal insulin response. It is possible that *APOE4* carriers who already exhibit insulin resistance in the brain may require moderate but long-lasting stimulation; thus, long-lasting insulin exposure might be beneficial. Future studies will be needed to further understand the mechanistic basis of *APOE* isoform-related differences upon insulin treatments in order to design individualized therapies for AD based on *APOE* genotype status.

Peripheral insulin resistance and dyslipidemia, the defining features of type 2 diabetes, exacerbate Aβ pathology and increase tau phosphorylation in AD patients (Ho et al., 2004; Kim et al., 2009a). Increasing evidence suggests that the presence of *APOE4* allele and type 2 diabetes synergistically affects AD pathogenesis. For example, individuals with both diabetes and *APOE4* have the highest risk for AD and exhibit the most severe neuropathology (Peila et al., 2002). In our study, HFD-induced peripheral insulin resistance led to accelerated insulin signaling defects from old to middle ages, suggesting that peripheral insulin resistance is a critical factor that accelerates apoE4-induced impairment of cerebral insulin signaling. Previous studies showed that insulin resistance promotes vascular dysfunction and dyslipidemia, which further exacerbate glucose and lipid abnormalities (Craft, 2009), resulting in a vicious cycle between progressive vascular dysfunction and enhanced insulin resistance. Thus, it is possible that apoE4 exacerbates insulin resistance by modulating lipid metabolism and vascular functions in the brain. Further understanding on the molecular mechanisms by which apoE4 and peripheral insulin resistance synergistically increase the risk of AD will help develop therapeutic strategy to treat this disease.

According to previous clinical findings, apoE4 status is not associated with the risk of type 2 diabetes (Anthopoulos et al., 2010). In our study, we detected a decreased signaling activation in the skeletal muscle of aged apoE4-TR mice upon acute peripheral stimulation of high-dose insulin, whereas the basal signaling in both skeletal muscle and liver at the steady state did not significantly differ between aged apoE3- and apoE4-TR mice. These results suggest that the peripheral system may possess certain compensation mechanism which allows the basal insulin signaling to be maintained under the physiological condition. In addition, peripheral and cerebral apoE may have different functions (Zhao et al., 2017). ApoE is mainly produced by hepatocytes and macrophages in the peripheral tissues, whereas in the CNS, apoE is highly expressed by astrocytes (Xu et al., 2006). The blood-brain barrier limits the transport of apoE into and out of the brain such that peripheral and cerebral apoE molecules are in separate pools (Lane-Donovan et al., 2016). The plasma apoE is desialylated and preferentially associated with very low-density lipoprotein particles, whereas the apoE in the CNS is found in high-density lipoprotein (HDL)-like particles (Kim et al., 2009b). These observations suggest that peripheral and brain apoE proteins exhibit distinct lipidation status, post-translational modifications and functions, which may contribute to the differential effects of apoE isoforms on the regulation of insulin signaling in the periphery and CNS. Future studies are required to investigate the different regulatory pathways of insulin signaling in the CNS and periphery.

We previously revealed that LRP1 interacts with IR in the brain and regulates insulin signaling (Liu et al., 2015). LRP1 could also regulate hepatic insulin response (Ding et al., 2016). As LRP1 is a major apoE receptor, we examined whether apoE4 affects the trafficking of LRP1. We found that apoE4 suppresses cell surface IR, but has no effect on cell surface LRP1 levels. In addition, our *in vitro* and *in vivo* results showed that apoE4 is capable of binding to IR, and such interaction becomes more pronounced in aged apoE4-TR mice, implying that apoE4 can directly modulate insulin signaling. However, as both apoE4 and LRP1 can bind to IR, we cannot rule out the possibility that they have competing or synergistic effects on the regulation of insulin signaling. Further investigations are necessary to define the role of LRP1 in apoE isoform-regulated insulin signaling.

In summary, our study not only reveals an age-dependent deleterious effects of apoE4 that is further accelerated by peripheral insulin resistance conditions but also uncovers an underlying molecular mechanism by which apoE4 retains IR in the endosomes. We believe that the potentially aggregative behavior of apoE4 is responsible for several pathogenic effects of apoE4 including trapping functional receptors in non-productive compartments. Gaining a better understanding on the mechanisms of apoE-regulated insulin signaling should enhance our understanding about why *APOE4* is a strong risk factor for cognitive decline and AD, and teach us about how we can target apoE in an isoform-specific manner to improve cerebral insulin signaling to treat AD.

## STAR METHODS

### CONTACT FOR REAGENT AND RESOURCE SHARING

Further information and requests for resources and reagents should be directed to and will be fulfilled by the Lead Contact, Dr. Guojun Bu (bu.guojun@mayo.edu).

### EXPERIMENTAL MODEL AND SUBJECT DETAILS

**Animals—**All animal procedures were approved by the Mayo Clinic Institutional Animal Care and Use Committee (IACUC) and were in accordance with the National Institutes of Health Guide for the Care and Use of Laboratory Animals. ApoE-targeted replacement (apoE-TR) mice in which murine *Apoe* gene locus is replaced with human *APOE3* or *APOE4* gene were obtained from Taconic. Animals were housed under controlled conditions of temperature and lighting and given free access to food and water. Male and female apoE-TR mice at 3, 12 and 22 months of age were used in glucose metabolism and insulin signaling experiments.

In HFD treatment experiments, 8-month-old male and female apoE3- and apoE4-TR mice were kept on a high fat (60% fat, Research Diets, D12492) or normal fat diet (5.8%, Harlan Laboratories, 7012) for 4 months. The body weight of the mice was evaluated every month during the experiments. Fasting blood glucose levels were examined using a blood glucose meter at the end of the experiment (Nipro Diagnostics).

***In vivo* Brain Insulin Delivery by Reverse Microdialysis—**Insulin (100 μIU/min, Sigma) was administrated into the left hippocampus of the 22-month-old apoE-TR mice or HFD-treated apoE-TR mice via *in vivo* reverse microdialysis as described (Liu et al., 2015).

Mice were anesthetized with 1%–2% isoflurane, and guide cannula (CMA Microdialysis or Bioanalytical Systems) were surgically implanted into the hippocampus (3.1 mm behind bregma, 2.5 mm lateral to midline, and 1.2 mm below dura at a 12° angle) using a standard stereotaxic frame (Kopf). Mice were allowed to recover for 24 hours. Microdialysis experiments were performed on conscious, freely moving mice. Mice were fasted overnight before the experiment. On the day of the experiment, the stylet in the guide cannula was replaced with the microdialysis probe. Probes of 30 kDa molecular weight cutoff membrane (Bioanalytical Systems) were used. The probe was perfused at 2 μl/min with aCSF (145 mM NaCl, 1.2 mM $CaCl_2$, 3 mM KCl, and 1.0 mM $MgCl_2$) for a 2 hours equilibration period before insulin delivery. HFD-treated mice were harvested after 1 hour of insulin treatment and the brain lysates were analyzed by Western blotting. The 22-month-old apoE-TR mice were harvested after four hours of treatment to examine insulin signaling activation, and the brain lysates were analyzed by Western blotting.

**Animals and Brain Tissue Preparation—**For tissue preparation, mice were transcardially perfused with saline. Different regions of brain tissues (cortex and hippocampus) were frozen on dry ice and stored at −80°C. For biochemical analysis, the brain tissues were homogenized and lysed with RIPA buffer (Thermo Fisher Scientific) containing protease inhibitor cocktail and phosphatase inhibitor (Roche), and centrifuged at 40,000 g for 60 minutes at 4°C. The supernatants were collected as RIPA fractions. The pellets were resuspended in guanidine-HCl (GND, 5 M) and centrifuged at 40,000 g for 60 minutes at 4°C. The supernatants were collected as GND fractions (Liu et al., 2016). All fractions were stored in −80°C until used for Western blot and ELISA analysis.

***In Vivo* Peripheral Insulin Delivery and Tissue Preparation—**The apoE-TR mice (22 months of age) with overnight fasting were anesthetized by intraperitoneal administration of Ketamine/Xylazine cocktail, and insulin (5 U, Sigma) was injected through the inferior vena cava. The hindlimb muscles (gluteus and soleus) were removed 4 minutes after insulin injection, and were homogenized and lysed in RIPA buffer (Thermo Fisher Scientific) containing protease inhibitor cocktail and phosphatase inhibitor (Roche). The resulting supernatants were used for Western blot analysis.

**Primary Neuron Culture and Treatment Paradigm of ApoE and Insulin—**Primary mouse cortical neurons were obtained from 16–18 d embryos of *Apoe*$^{-/-}$ mice. Cultures were grown in neurobasal medium supplemented with B27 (Thermo Fisher Scientific), 0.5 mM glutamine, 100 U/ml penicillin and 100 g/ml streptomycin. Neurons were seeded at a density of $10^6$ cells/per well in 6-well plates or $3 \times 10^4$ cells/per well in 96-well plates. At 5 days in vitro (DIV), the cells were treated with cytosine arabinofuranoside (Ara-C, Sigma) to eliminate glia cells. At DIV10, the cells were treated overnight with 50 nM recombinant apoE (Fitzgerald) in neurobasal medium supplemented with B27 minus insulin (Thermo Fisher Scientific). Insulin was administrated for half an hour at a concentration of 100 nM before harvesting the cells for insulin signaling analysis by Western blotting.

**ApoE and Insulin Treatment in HuH7 Cells—**HuH7 cells were seeded at a density of $0.5 \times 10^6$ cells/per well in 6-well plates and treated overnight with 50 nM recombinant apoE

(Fitzgerald) in serum-free DMEM medium. Insulin was administrated for 5, 15, 30 or 60 minutes at a concentration of 100 nM before cells were harvested for insulin signaling analysis by Western blotting.

**Purification of Lipidated ApoE from Culture Medium—**Immortalized mouse astrocytes derived from apoE3-TR and apoE4-TR mice were cultured as described previously (Morikawa et al., 2005). Culture medium was conditioned with serum-free medium for 36~48 hours. Conditioned medium was concentrated using Amicon centrifugal filter unit (Millipore), and run through HiTrap Heparin column on an AKTA FPLC system (GE Healthcare). Heparin-bound apoE was eluted with NaCl gradient from 0 to 1 M in Tris buffer. Cholesterol concentration was detected for each fraction by the Amplex Red Cholesterol Assay kit (Thermo Fisher). The peak fractions containing apoE that is associated with cholesterol were concentrated. The concentration and purity of apoE was quantified by apoE ELISA as (Fu et al., 2016).

**Measurement of Mitochondrial Respiration and Glycolysis—**Mitochondrial respiration and glycolysis were measured by directly detecting oxygen consumption (OCR) and extracellular acidification rate (ECAR) respectively using a Seahorse XF96 Extracellular Flux analyzer (Seahorse Bioscience). Cortical neurons form *Apoe*$^{-/-}$ mice were seeded into Seahorse XF96-well plates at a density of 30,000 cells per well. At DIV8, one day before seahorse experiment, the cells were treated with 50 nM recombinant or lipidated apoE isoforms for overnight in neurobasal medium supplemented with B27 minus insulin. Sensor cartridges were hydrated in XF calibrant and maintained at 37°C in air without $CO_2$ one day before the experiment. The mitochondrial stress test was performed according to the Seahorse Bioscience protocol. In brief, on the day of the mitochondria stress tests, cells were treated with 100 nM insulin for 30 minutes and then washed once and incubated with bicarbonate-free low-buffered assay medium (glucose 10 mM, glutamine 2 mM, sodium pyruvate 1 mM, pH adjusted to 7.4 with NaOH) for one hour at 37°C in the absence of $CO_2$ prior to the beginning of the assay. Changes in cellular respiration were assessed over time after sequential injections of 2 μM oligomycin in port A, 1 μM FCCP in port B and 5 μM rotenone/antimycin A in port C. Three measurements were performed in each session at 3 minute intervals. From the mitochondrial assay we determined the following parameters: the basal respiration (average OCR of three measurements preceding oligomycin injection), and the maximal respiration (average OCR of three measurements between FCCP and before rotenone/antimycin A injection).

The glycolysis stress test was performed according to the Seahorse Bioscience protocol. Briefly, on the day of the experiment cells were washed once and incubated with bicarbonate-free low-buffered glycolysis assay medium (glucose-free, glutamine 2 mM, pH adjusted to 7.4 with NaOH) for one hour at 37°C in the absence of $CO_2$ prior to the beginning of the assay. The glycolysis stress test employed in the present study used sequential injections of glucose (10 mM, port A), oligomycin (2 μM, port B) and 2-deoxyglucose (50 mM, port C). Three measurements were performed in each session at 3 minute intervals. From the glycolysis assay we determined the following parameters: the glycolysis rate (average ECAR of three measurements between glucose and oligomycin

injection), and the glycolytic capacity (average ECAR of three measurements between oligomycin and 2-deoxyglucose injection).

**Cell Surface Biotinylation—**At DIV10, primary neurons from *Apoe*$^{-/-}$ mice were treated overnight with 100 nM recombinant apoE with or without insulin for 30 minutes at 37°C. Neurons were washed with cold PBS once and then incubated in PBS containing 0.5 mg/mL sulfo-NHS-SS-biotin (Pierce) for 30 minutes at 4°C with shaking. Excess reagent was quenched by rinsing in cold PBS containing 50 mM glycine. Cells were lysed with RIPA containing protease inhibitor cocktail for 20 minutes at 4°C. Cell lysate was collected and centrifuged at 10,000 × g for 10 minutes. After protein quantification with BCA kit (Pierce), the cell lysates with same amount of protein was incubated with 100 μL of NeutrAvidin agarose (Pierce) at 4°C for 2 hours. Agarose beads were washed three times in PBS contained with protease inhibitor cocktail. Biotinylated surface proteins and total proteins were analyzed by Western blotting.

**Truncated apoE preparation—**The full-length or C-terminal truncated apoE3 and apoE4 were subcloned and inserted into a pcDNA3.1(+) vector between HindIII and XhoI sites. HEK293T cells cultured in DMEM high glucose containing 10% FBS and penicillin/streptomycin were transfected with the plasmids using polyethylenimine (PEI). Twenty-four hours after the transfection, culture medium was changed to serum-free DMEM and conditioned for 36~48 hours. The conditioned medium was concentrated and run through a HiTrap heparin column on an AKTA FPLC system (GE Healthcare). Heparin-bound apoE was eluted with 0 to 1 M gradient of NaCl. The peak fractions containing apoE were concentrated, and quantified by immunoblot with a monoclonal anti-apoE antibody.

**Solid-phase Binding Assay—**Recombinant apoE3 or apoE4, astrocyte-secreted lipidated apoE3 or apoE4 particles, C-terminal truncated apoE3 or apoE4, and recombinant apoJ were coated into 96-well plate (400 ng/well) overnight at 4°C. After washing and blocking with ACE blocking buffer (AbD Serotec) for 3 hours at room temperature, biotinylated human insulin (Eagle Biosciences) or human IR (R&D Systems) at a concentration between 0 to 700 nM (in PBS containing 1% BSA) were added and incubated for 24 hours at 4°C. After washing, biotinylated insulin was detected with poly-avidin-HRP (Fitzgerald Industries) for 1 hour at room temperature. IR was detected by incubating with biotinylated anti-human IR antibody (R&D Systems) for 2 hours at room temperature, followed by poly-avidin-HRP (Fitzgerald Industries) for 1 hour at room temperature. After washing, the ELISA assays were developed using Super Slow ELISA TMB (Sigma) with absorbance read on a Bio-Tek plate reader. To establish the working condition of insulin and IR interaction, recombinant biotinylated human insulin (8 nM) and recombinant IR (at a concentration between 0 to 300 nM) were incubated in 96-well plate at 37°C for 1 hour. To test whether apoE could compete the interaction of insulin and IR, recombinant apoE3 or apoE4 (4, 8, or 16 μg/ml) was mixed with biotinylated human insulin (8 nM) and recombinant IR (80 nM) and incubated at 37°C for 1 hour. The mixed solution was transferred into Streptavidin Coated plate (R&D Systems) and incubated at 4°C for 24 hours. After washing the plate, mouse anti-human IR antibody (R&D Systems) was added and incubated at room temperature for 2 hours. Plates were washed and then incubated with

anti-mouse IgG-HRP antibody (GE Healthcare) for 2 hours at room temperature. The ELISA assays were developed using Super Slow ELISA TMB (Sigma) with absorbance read on a Bio-Tek plate reader.

**Solution Binding Assay and Co-immunoprecipitation—**Recombinant human apoE protein (1 μM, Fitzgerald) and IR protein (400 nM, R&D Systems) were incubated for 1 hour at 37°C in 20 μl of phosphate-buffered saline at neutral pH. The solution complex was immunoprecipitated overnight at 4°C using the biotin-conjugated mouse monoclonal apoE antibody (K74180B, Meridian Life Science) or biotin-conjugated rabbit IgG (Thermo Fisher Scientific) as control. The antibody-bound complexes were isolated by incubation with Avidin-agarose beads (Thermo Fisher Scientific). The precipitates were then washed three times with PBS and resuspended in SDS sample buffer. The amount of apoE and IR was detected by Western blotting by using the following antibodies: anti-apoE (WUE4, Novus) and anti-IR (Santa Cruz Biotechnology).

**Transfection of IR-GFP Plasmids and Confocal Microscopy—**SH-SY5Y cells were cultured on 8-well chamber (Ibidi) for 24 hours and then transfected with human IR tagged with GFP (IR-GFP) plasmids (Addgene Plasmid #22286) using Lipofectamine 3000 (Thermo Fisher Scientific) according to the manufacturer's instructions. Twenty-four hours after transfection, cells were treated overnight with recombinant apoE3 or apoE4 proteins at a concentration of 100 nM. Cells were incubated with Alexa568-labeled human transferrin (Tf) or Lysotracker Red DND99 (Thermo Fisher Scientific) for one hour and stimulated with insulin (100 nM) at 30 minutes before fixation. After fixing with 4% PFA, cells were observed by a confocal laser-scanning fluorescence microscope (Carl Zeiss). The co-localization of proteins was quantified by ImageJ software (National Institutes of Health), and the Manders' coefficient was calculated with JACoP (rsbweb.nih.gov/ij/plugins/track/jacop. html).

**Endocytosis Assay—**IR endocytosis was performed to detect the changes of internalized IR labeled with cleavable biotin as described (Cihil and Swiatecka-Urban, 2013; Ehlers, 2000). The *Apoe*$^{-/-}$ primary neurons were incubated in PBS containing 1 mg/mL sulfo-NHS-SS-biotin (Pierce) for 15 minutes at 4°C with shaking to label the cell surface proteins. The cells were then treated with recombinant apoE (100 nM) in the presence or absence of insulin (100 nM) at 37°C for various times to allow IR trafficking to occur. The remaining surface biotin was then removed by reducing its disulfide linkage with glutathione cleavage buffer (50 mM glutathione in 75 mM NaCl and 10 mM EDTA containing 1% BSA and 0.075 N NaOH). The internalized (biotinylated) receptors were isolated by precipitation with streptavidin-conjugated beads, and IR was detected by Western blotting analysis with an anti-IR antibody (Millipore). The internalized IR was determined by measuring the band intensity at different time points and subtracting the band intensity at time zero.

**Recycling Assay—**IR recycling was measured by the loss of internalized IR labeled with cleavable biotin (Cihil and Swiatecka-Urban, 2013; Ehlers, 2000). Surface IR of cortical *Apoe*$^{-/-}$ neurons was biotinylated at 4°C as above and the cells were then treated with recombinant apoE proteins (100 nM) at 37°C for 30 minutes to allow IR endocytosis to

occur. Cells were then cooled at 4°C to stop endocytic trafficking and the cell surface biotin were removed by glutathione cleavage buffer (two times for 15 minutes each). The cells were then returned to growth media at 37°C for various times to allow the recycling of internalized receptors. The cells were then cooled to 4°C and incubated with glutathione cleavage buffer to ensure complete removal of any newly appeared surface biotin. Residual biotinylated (internalized) receptors were then isolated by streptavidin precipitation, and IR was detected by Western blotting with an anti-IR antibody (Millipore). The internalized IR was determined by measuring the percentage of the band intensity at different time points to the band intensity at time zero. The reduction of intracellular IR provides a measure of receptor recycling.

**IR and ApoE ELISA—**Levels of IR and apoE were determined by ELISAs. IR ELISA was performed according to the manufacturer instructions (LifeSpan BioSciences). For apoE ELISA, WUE4 capture antibody (Novus) and biotin-conjugated mouse monoclonal K74180B detector antibody (Meridian Life Science) were used as described (Fu et al., 2016). Recombinant human apoE3 and apoE4 (Fitzgerald) were used as standard. Colorimetric quantification was performed on a Synergy HT plate reader (BioTek) using horseradish peroxidase (HRP)-linked streptavidin (Vector) and Super Slow ELISA TMB (Sigma).

**Histology and Immunohistochemistry—**The hemibrain of apoE-TR mice fixed in 10% formalin was embedded in paraffin wax, sectioned in a coronal plane at 5 micron thickness and mounted on glass slides. The tissue sections were deparaffinized in xylene and rehydrated in a graded series of alcohols. Antigen retrieval was performed by steaming in Tris-EDTA buffer (Abcam) for 30 minutes, and endogenous peroxidase activity was blocked by incubation in 0.03% hydrogen peroxide. Sections were then immunostained with Rab5 antibody (Abcam) by using the DAKO Autostainer (DAKO North America, Carpinteria, CA) and the DAKO EnVision+HRP system. The stained slides were then dehydrated, cover-slipped, scanned with the Aperio Slide Scanner (Aperio, Vista, CA), and analyzed with Aperio ImageScope.

**Western Blotting and Co-immunoprecipitation—**Equal amounts of protein from the homogenized tissue lysates or cell lysates were resolved by SDS-PAGE and transferred to PVDF membranes. After the membranes were blocked, proteins were detected with primary antibody. Membrane was probed with LI-COR IRDye secondary antibodies and detected using the Odyssey infrared imaging system (LI-COR). In some experiments, HRP-conjugated secondary antibody was visualized by ECL detection system (Pierce) and exposed to film. The following antibodies were used in this study: anti-phospho-Ser473-Akt (p-Akt, Cell Signaling Technology), anti-Akt (Cell Signaling Technology), anti-phospho-Ser9-GSK3β (p-GSK3β, Cell Signaling Technology), anti-GSK3β (Cell Signaling Technology), anti-phospho-Tyr1345 IR (p-IR, Cell Signaling Technology), anti-IR (SantaCruz Biotechnology), anti-apoE antibodies (Meridian Life Science), anti-LRP1 antibody [in-house, (Bu et al., 1995)], anti-NMDAR(NR2B) antibody (Millipore), anti-AMPAR(GluR2) antibody (Millipore), anti-Na-K-ATPase antibody(Abcam), and anti-β-actin (Sigma) antibodies.

For IR immunoprecipitation, the brain lysates were pre-cleared using Protein A-agarose beads (ThermoFisher Scientific) for 30 minutes at 4°C and immunoprecipitated overnight at 4°C using anti-IR antibody (Santa Cruz Biotechnology) and Protein A-agarose beads. The precipitates were then washed three times with PBS and resuspended in SDS sample buffer for Western blotting. ApoE immunoprecipitation was performed by using the biotin-conjugated mouse monoclonal apoE antibody (K74180B, Meridian Life Science) and Avidin-agarose beads (ThermoFisher Scientific).

**Statistical Analysis—**Comparisons between two groups were performed with Student's *t* tests, and those among more than two groups were performed with ANOVA. A p value of $< 0.05$ was considered statistically significant.

## Supplementary Material

Refer to Web version on PubMed Central for supplementary material.

## Acknowledgments

This work was supported by NIH grants R01AG035355, R01AG027924, RF1AG051504, and R01AG046205 (to GB), a grant from the Cure Alzheimer's Fund (to GB), a fellowship from the BrightFocus Foundation (to C-CL), a pilot project grant from Mayo Clinic Alzheimer's Disease Research Center (to NZ), and Younkin fellowship from Mayo Clinic (to NZ). We thank Linda Rousseau and Monica Castanedes-Casey for helping with the preparation of mouse brain slices and the immunohistochemical staining.

## References

Aleshkov S, Abraham CR, Zannis VI. Interaction of nascent ApoE2, ApoE3, and ApoE4 isoforms expressed in mammalian cells with amyloid peptide beta (1–40). Relevance to Alzheimer's disease. Biochemistry. 1997; 36:10571–10580. [PubMed: 9265639]

Anthopoulos PG, Hamodrakas SJ, Bagos PG. Apolipoprotein E polymorphisms and type 2 diabetes: a meta-analysis of 30 studies including 5423 cases and 8197 controls. Mol Genet Metab. 2010; 100:283–291. [PubMed: 20381392]

Baldwin D Jr, Prince M, Marshall S, Davies P, Olefsky JM. Regulation of insulin receptors: evidence for involvement of an endocytotic internalization pathway. Proc Natl Acad Sci U S A. 1980; 77:5975–5978. [PubMed: 6108561]

Beitner R, Kalant N. Stimulation of glycolysis by insulin. J Biol Chem. 1971; 246:500–503. [PubMed: 5542017]

Biessels GJ, Staekenborg S, Brunner E, Brayne C, Scheltens P. Risk of dementia in diabetes mellitus: a systematic review. Lancet Neurol. 2006; 5:64–74. [PubMed: 16361024]

Bomfim TR, Forny-Germano L, Sathler LB, Brito-Moreira J, Houzel JC, Decker H, Silverman MA, Kazi H, Melo HM, McClean PL, et al. An anti-diabetes agent protects the mouse brain from defective insulin signaling caused by Alzheimer's disease- associated Abeta oligomers. J Clin Invest. 2012; 122:1339–1353. [PubMed: 22476196]

Bu G. Apolipoprotein E and its receptors in Alzheimer's disease: pathways, pathogenesis and therapy. Nat Rev Neurosci. 2009; 10:333–344. [PubMed: 19339974]

Bu G, Geuze HJ, Strous GJ, Schwartz AL. 39 kDa receptor-associated protein is an ER resident protein and molecular chaperone for LDL receptor-related protein. EMBO J. 1995; 14:2269–2280. [PubMed: 7774585]

Calero M, Rostagno A, Matsubara E, Zlokovic B, Frangione B, Ghiso J. Apolipoprotein J (clusterin) and Alzheimer's disease. Microsc Res Tech. 2000; 50:305–315. [PubMed: 10936885]

Carpentier JL, Gorden P, Amherdt M, Van Obberghen E, Kahn CR, Orci L. 125I-insulin binding to cultured human lymphocytes. Initial localization and fate of hormone determined by quantitative electron microscopic autoradiography. J Clin Invest. 1978; 61:1057–1070. [PubMed: 659578]

Cataldo AM, Peterhoff CM, Troncoso JC, Gomez-Isla T, Hyman BT, Nixon RA. Endocytic pathway abnormalities precede amyloid beta deposition in sporadic Alzheimer's disease and Down syndrome: differential effects of APOE genotype and presenilin mutations. Am J Pathol. 2000; 157:277–286. [PubMed: 10880397]

Chan ES, Chen C, Cole GM, Wong BS. Differential interaction of Apolipoprotein-E isoforms with insulin receptors modulates brain insulin signaling in mutant human amyloid precursor protein transgenic mice. Sci Rep. 2015; 5:13842. [PubMed: 26346625]

Chan ES, Shetty MS, Sajikumar S, Chen C, Soong TW, Wong BS. ApoE4 expression accelerates hippocampus-dependent cognitive deficits by enhancing Abeta impairment of insulin signaling in an Alzheimer's disease mouse model. Sci Rep. 2016; 6:26119. [PubMed: 27189808]

Chen Y, Durakoglugil MS, Xian X, Herz J. ApoE4 reduces glutamate receptor function and synaptic plasticity by selectively impairing ApoE receptor recycling. Proc Natl Acad Sci U S A. 2010; 107:12011–12016. [PubMed: 20547867]

Cihil KM, Swiatecka-Urban A. The cell-based L-glutathione protection assays to study endocytosis and recycling of plasma membrane proteins. J Vis Exp. 2013:e50867. [PubMed: 24378656]

Claxton A, Baker LD, Hanson A, Trittschuh EH, Cholerton B, Morgan A, Callaghan M, Arbuckle M, Behl C, Craft S. Long-acting intranasal insulin detemir improves cognition for adults with mild cognitive impairment or early-stage Alzheimer's disease dementia. J Alzheimers Dis. 2015; 44:897–906. [PubMed: 25374101]

Claxton A, Baker LD, Wilkinson CW, Trittschuh EH, Chapman D, Watson GS, Cholerton B, Plymate SR, Arbuckle M, Craft S. Sex and ApoE genotype differences in treatment response to two doses of intranasal insulin in adults with mild cognitive impairment or Alzheimer's disease. J Alzheimers Dis. 2013; 35:789–797. [PubMed: 23507773]

Cohen P, Frame S. The renaissance of GSK3. Nat Rev Mol Cell Biol. 2001; 2:769–776. [PubMed: 11584304]

Craft S. The role of metabolic disorders in Alzheimer disease and vascular dementia: two roads converged. Arch Neurol. 2009; 66:300–305. [PubMed: 19273747]

Craft S, Asthana S, Schellenberg G, Baker L, Cherrier M, Boyt AA, Martins RN, Raskind M, Peskind E, Plymate S. Insulin effects on glucose metabolism, memory, and plasma amyloid precursor protein in Alzheimer's disease differ according to apolipoprotein-E genotype. Ann N Y Acad Sci. 2000; 903:222–228. [PubMed: 10818510]

Craft S, Cholerton B, Baker LD. Insulin and Alzheimer's disease: untangling the web. J Alzheimers Dis. 2013; 33(Suppl 1):S263–275. [PubMed: 22936011]

Craft S, Watson GS. Insulin and neurodegenerative disease: shared and specific mechanisms. Lancet Neurol. 2004; 3:169–178. [PubMed: 14980532]

David DC, Ollikainen N, Trinidad JC, Cary MP, Burlingame AL, Kenyon C. Widespread protein aggregation as an inherent part of aging in C. elegans. PLoS Biol. 2010; 8:e1000450. [PubMed: 20711477]

De Felice FG, Ferreira ST. Inflammation, defective insulin signaling, and mitochondrial dysfunction as common molecular denominators connecting type 2 diabetes to Alzheimer disease. Diabetes. 2014; 63:2262–2272. [PubMed: 24931033]

DeFronzo RA, Tripathy D. Skeletal muscle insulin resistance is the primary defect in type 2 diabetes. Diabetes Care. 2009; 32(Suppl 2):S157–163. [PubMed: 19875544]

Di Guglielmo GM, Drake PG, Baass PC, Authier F, Posner BI, Bergeron JJ. Insulin receptor internalization and signalling. Mol Cell Biochem. 1998; 182:59–63. [PubMed: 9609114]

Ding Y, Xian X, Holland WL, Tsai S, Herz J. Low-Density Lipoprotein Receptor-Related Protein-1 Protects Against Hepatic Insulin Resistance and Hepatic Steatosis. EBioMedicine. 2016; 7:135–145. [PubMed: 27322467]

Ehlers MD. Reinsertion or degradation of AMPA receptors determined by activity-dependent endocytic sorting. Neuron. 2000; 28:511–525. [PubMed: 11144360]

Elliott DA, Halliday GM, Garner B. Apolipoprotein-E forms dimers in human frontal cortex and hippocampus. BMC Neurosci. 2010; 11:23. [PubMed: 20170526]

Fu Y, Zhao J, Atagi Y, Nielsen HM, Liu CC, Zheng H, Shinohara M, Kanekiyo T, Bu G. Apolipoprotein E lipoprotein particles inhibit amyloid-beta uptake through cell surface heparan sulphate proteoglycan. Mol Neurodegener. 2016; 11:37. [PubMed: 27151330]

Garcia-Caceres C, Quarta C, Varela L, Gao Y, Gruber T, Legutko B, Jastroch M, Johansson P, Ninkovic J, Yi CX, et al. Astrocytic Insulin Signaling Couples Brain Glucose Uptake with Nutrient Availability. Cell. 2016; 166:867–880. [PubMed: 27518562]

Ginsberg SD, Mufson EJ, Counts SE, Wuu J, Alldred MJ, Nixon RA, Che S. Regional selectivity of rab5 and rab7 protein upregulation in mild cognitive impairment and Alzheimer's disease. J Alzheimers Dis. 2010; 22:631–639. [PubMed: 20847427]

Gorden P, Carpentier JL, Freychet P, LeCam A, Orci L. Intracellular translocation of iodine-125-labeled insulin: direct demonstration in isolated hepatocytes. Science. 1978; 200:782–785. [PubMed: 644321]

Grbovic OM, Mathews PM, Jiang Y, Schmidt SD, Dinakar R, Summers-Terio NB, Ceresa BP, Nixon RA, Cataldo AM. Rab5-stimulated up-regulation of the endocytic pathway increases intracellular beta-cleaved amyloid precursor protein carboxyl-terminal fragment levels and Abeta production. J Biol Chem. 2003; 278:31261–31268. [PubMed: 12761223]

Hatters DM, Zhong N, Rutenber E, Weisgraber KH. Amino-terminal domain stability mediates apolipoprotein E aggregation into neurotoxic fibrils. J Mol Biol. 2006; 361:932–944. [PubMed: 16890957]

Heeren J, Grewal T, Laatsch A, Becker N, Rinninger F, Rye KA, Beisiegel U. Impaired recycling of apolipoprotein E4 is associated with intracellular cholesterol accumulation. J Biol Chem. 2004; 279:55483–55492. [PubMed: 15485881]

Ho L, Qin W, Pompl PN, Xiang Z, Wang J, Zhao Z, Peng Y, Cambareri G, Rocher A, Mobbs CV, et al. Diet-induced insulin resistance promotes amyloidosis in a transgenic mouse model of Alzheimer's disease. FASEB J. 2004; 18:902–904. [PubMed: 15033922]

Hoyer S. Glucose metabolism and insulin receptor signal transduction in Alzheimer disease. Eur J Pharmacol. 2004; 490:115–125. [PubMed: 15094078]

Jack CR Jr, Knopman DS, Jagust WJ, Shaw LM, Aisen PS, Weiner MW, Petersen RC, Trojanowski JQ. Hypothetical model of dynamic biomarkers of the Alzheimer's pathological cascade. Lancet Neurol. 2010; 9:119–128. [PubMed: 20083042]

Kim B, Backus C, Oh S, Hayes JM, Feldman EL. Increased tau phosphorylation and cleavage in mouse models of type 1 and type 2 diabetes. Endocrinology. 2009a; 150:5294–5301. [PubMed: 19819959]

Kim J, Basak JM, Holtzman DM. The role of apolipoprotein E in Alzheimer's disease. Neuron. 2009b; 63:287–303. [PubMed: 19679070]

Kublaoui B, Lee J, Pilch PF. Dynamics of signaling during insulin-stimulated endocytosis of its receptor in adipocytes. J Biol Chem. 1995; 270:59–65. [PubMed: 7814420]

Lane-Donovan C, Philips GT, Herz J. More than cholesterol transporters: lipoprotein receptors in CNS function and neurodegeneration. Neuron. 2014; 83:771–787. [PubMed: 25144875]

Lane-Donovan C, Wong WM, Durakoglugil MS, Wasser CR, Jiang S, Xian X, Herz J. Genetic Restoration of Plasma ApoE Improves Cognition and Partially Restores Synaptic Defects in ApoE-Deficient Mice. J Neurosci. 2016; 36:10141–10150. [PubMed: 27683909]

Lindner AB, Demarez A. Protein aggregation as a paradigm of aging. Biochim Biophys Acta. 2009; 1790:980–996. [PubMed: 19527771]

Liu CC, Hu J, Tsai CW, Yue M, Melrose HL, Kanekiyo T, Bu G. Neuronal LRP1 regulates glucose metabolism and insulin signaling in the brain. J Neurosci. 2015; 35:5851–5859. [PubMed: 25855193]

Liu CC, Kanekiyo T, Xu H, Bu G. Apolipoprotein E and Alzheimer disease: risk, mechanisms and therapy. Nat Rev Neurol. 2013; 9:106–118. [PubMed: 23296339]

Liu CC, Zhao N, Yamaguchi Y, Cirrito JR, Kanekiyo T, Holtzman DM, Bu G. Neuronal heparan sulfates promote amyloid pathology by modulating brain amyloid-beta clearance and aggregation in Alzheimer's disease. Sci Transl Med. 2016; 8:332ra344.

Martel CL, Mackic JB, Matsubara E, Governale S, Miguel C, Miao W, McComb JG, Frangione B, Ghiso J, Zlokovic BV. Isoform-specific effects of apolipoproteins E2, E3, and E4 on cerebral capillary sequestration and blood-brain barrier transport of circulating Alzheimer's amyloid beta. J Neurochem. 1997; 69:1995–2004. [PubMed: 9349544]

Michael MD, Kulkarni RN, Postic C, Previs SF, Shulman GI, Magnuson MA, Kahn CR. Loss of insulin signaling in hepatocytes leads to severe insulin resistance and progressive hepatic dysfunction. Mol Cell. 2000; 6:87–97. [PubMed: 10949030]

Morikawa M, Fryer JD, Sullivan PM, Christopher EA, Wahrle SE, DeMattos RB, O'Dell MA, Fagan AM, Lashuel HA, Walz T, et al. Production and characterization of astrocyte-derived human apolipoprotein E isoforms from immortalized astrocytes and their interactions with amyloid-beta. Neurobiol Dis. 2005; 19:66–76. [PubMed: 15837562]

Morrow JA, Hatters DM, Lu B, Hochtl P, Oberg KA, Rupp B, Weisgraber KH. Apolipoprotein E4 forms a molten globule. A potential basis for its association with disease. J Biol Chem. 2002; 277:50380–50385. [PubMed: 12393895]

Nisr RB, Affourtit C. Insulin acutely improves mitochondrial function of rat and human skeletal muscle by increasing coupling efficiency of oxidative phosphorylation. Biochim Biophys Acta. 2014; 1837:270–276. [PubMed: 24212054]

Nixon RA. Endosome function and dysfunction in Alzheimer's disease and other neurodegenerative diseases. Neurobiol Aging. 2005; 26:373–382. [PubMed: 15639316]

Ong QR, Chan ES, Lim ML, Cole GM, Wong BS. Reduced phosphorylation of brain insulin receptor substrate and Akt proteins in apolipoprotein-E4 targeted replacement mice. Sci Rep. 2014; 4:3754. [PubMed: 24435134]

Ott A, Stolk RP, van Harskamp F, Pols HA, Hofman A, Breteler MM. Diabetes mellitus and the risk of dementia: The Rotterdam Study. Neurology. 1999; 53:1937–1942. [PubMed: 10599761]

Peila R, Rodriguez BL, Launer LJ. Type 2 diabetes, APOE gene, and the risk for dementia and related pathologies: The Honolulu-Asia Aging Study. Diabetes. 2002; 51:1256–1262. [PubMed: 11916953]

Reger MA, Watson GS, Frey WH 2nd, Baker LD, Cholerton B, Keeling ML, Belongia DA, Fishel MA, Plymate SR, Schellenberg GD, et al. Effects of intranasal insulin on cognition in memory-impaired older adults: modulation by APOE genotype. Neurobiol Aging. 2006; 27:451–458. [PubMed: 15964100]

Reger MA, Watson GS, Green PS, Baker LD, Cholerton B, Fishel MA, Plymate SR, Cherrier MM, Schellenberg GD, Frey WH 2nd, Craft S. Intranasal insulin administration dose-dependently modulates verbal memory and plasma amyloid-beta in memory-impaired older adults. J Alzheimers Dis. 2008; 13:323–331. [PubMed: 18430999]

Reiman EM, Caselli RJ, Yun LS, Chen K, Bandy D, Minoshima S, Thibodeau SN, Osborne D. Preclinical evidence of Alzheimer's disease in persons homozygous for the epsilon 4 allele for apolipoprotein E. N Engl J Med. 1996; 334:752–758. [PubMed: 8592548]

Reiman EM, Chen K, Alexander GE, Caselli RJ, Bandy D, Osborne D, Saunders AM, Hardy J. Correlations between apolipoprotein E epsilon4 gene dose and brain-imaging measurements of regional hypometabolism. Proc Natl Acad Sci U S A. 2005; 102:8299–8302. [PubMed: 15932949]

Sims-Robinson C, Kim B, Rosko A, Feldman EL. How does diabetes accelerate Alzheimer disease pathology? Nat Rev Neurol. 2010; 6:551–559. [PubMed: 20842183]

Small GW, Mazziotta JC, Collins MT, Baxter LR, Phelps ME, Mandelkern MA, Kaplan A, La Rue A, Adamson CF, Chang L, et al. Apolipoprotein E type 4 allele and cerebral glucose metabolism in relatives at risk for familial Alzheimer disease. JAMA. 1995; 273:942–947. [PubMed: 7884953]

Steen E, Terry BM, Rivera EJ, Cannon JL, Neely TR, Tavares R, Xu XJ, Wands JR, de la Monte SM. Impaired insulin and insulin-like growth factor expression and signaling mechanisms in Alzheimer's disease--is this type 3 diabetes? J Alzheimers Dis. 2005; 7:63–80. [PubMed: 15750215]

Talbot K, Wang HY, Kazi H, Han LY, Bakshi KP, Stucky A, Fuino RL, Kawaguchi KR, Samoyedny AJ, Wilson RS, et al. Demonstrated brain insulin resistance in Alzheimer's disease patients is associated with IGF-1 resistance, IRS-1 dysregulation, and cognitive decline. J Clin Invest. 2012; 122:1316–1338. [PubMed: 22476197]

Trischitta V, Wong KY, Brunetti A, Scalisi R, Vigneri R, Goldfine ID. Endocytosis, recycling, and degradation of the insulin receptor. Studies with monoclonal antireceptor antibodies that do not activate receptor kinase. J Biol Chem. 1989; 264:5041–5046. [PubMed: 2466841]

Unger JW, Livingston JN, Moss AM. Insulin receptors in the central nervous system: localization, signalling mechanisms and functional aspects. Prog Neurobiol. 1991; 36:343–362. [PubMed: 1887067]

Weisgraber KH, Shinto LH. Identification of the disulfide-linked homodimer of apolipoprotein E3 in plasma. Impact on receptor binding activity. J Biol Chem. 1991; 266:12029–12034. [PubMed: 2050696]

Willette AA, Bendlin BB, Starks EJ, Birdsill AC, Johnson SC, Christian BT, Okonkwo OC, La Rue A, Hermann BP, Koscik RL, et al. Association of Insulin Resistance With Cerebral Glucose Uptake in Late Middle-Aged Adults at Risk for Alzheimer Disease. JAMA Neurol. 2015; 72:1013–1020. [PubMed: 26214150]

Winzell MS, Ahren B. The high-fat diet-fed mouse: a model for studying mechanisms and treatment of impaired glucose tolerance and type 2 diabetes. Diabetes. 2004; 53(Suppl 3):S215–219. [PubMed: 15561913]

Xu Q, Bernardo A, Walker D, Kanegawa T, Mahley RW, Huang Y. Profile and regulation of apolipoprotein E (ApoE) expression in the CNS in mice with targeting of green fluorescent protein gene to the ApoE locus. J Neurosci. 2006; 26:4985–4994. [PubMed: 16687490]

Xu W, Weissmiller AM, White JA 2nd, Fang F, Wang X, Wu Y, Pearn ML, Zhao X, Sawa M, Chen S, et al. Amyloid precursor protein-mediated endocytic pathway disruption induces axonal dysfunction and neurodegeneration. J Clin Invest. 2016; 126:1815–1833. [PubMed: 27064279]

Zhang J, Nuebel E, Wisidagama DR, Setoguchi K, Hong JS, Van Horn CM, Imam SS, Vergnes L, Malone CS, Koehler CM, Teitell MA. Measuring energy metabolism in cultured cells, including human pluripotent stem cells and differentiated cells. Nat Protoc. 2012; 7:1068–1085. [PubMed: 22576106]

Zhao N, Liu CC, Qiao W, Bu G. Apolipoprotein E, Receptors, and Modulation of Alzheimer's Disease. Biol Psychiatry. 2017

Zhao WQ, Lacor PN, Chen H, Lambert MP, Quon MJ, Krafft GA, Klein WL. Insulin receptor dysfunction impairs cellular clearance of neurotoxic oligomeric a{beta}. J Biol Chem. 2009; 284:18742–18753. [PubMed: 19406747]

## Highlights

- ApoE4 impairs cerebral insulin signaling in an age-dependent manner.
- Peripheral insulin resistance and apoE4 synergistically impairs insulin signaling.
- ApoE4 reduces insulin-IR interaction and impairs IR trafficking.
- ApoE4 aggregation and endosomal dysfunction impair insulin signaling with aging.

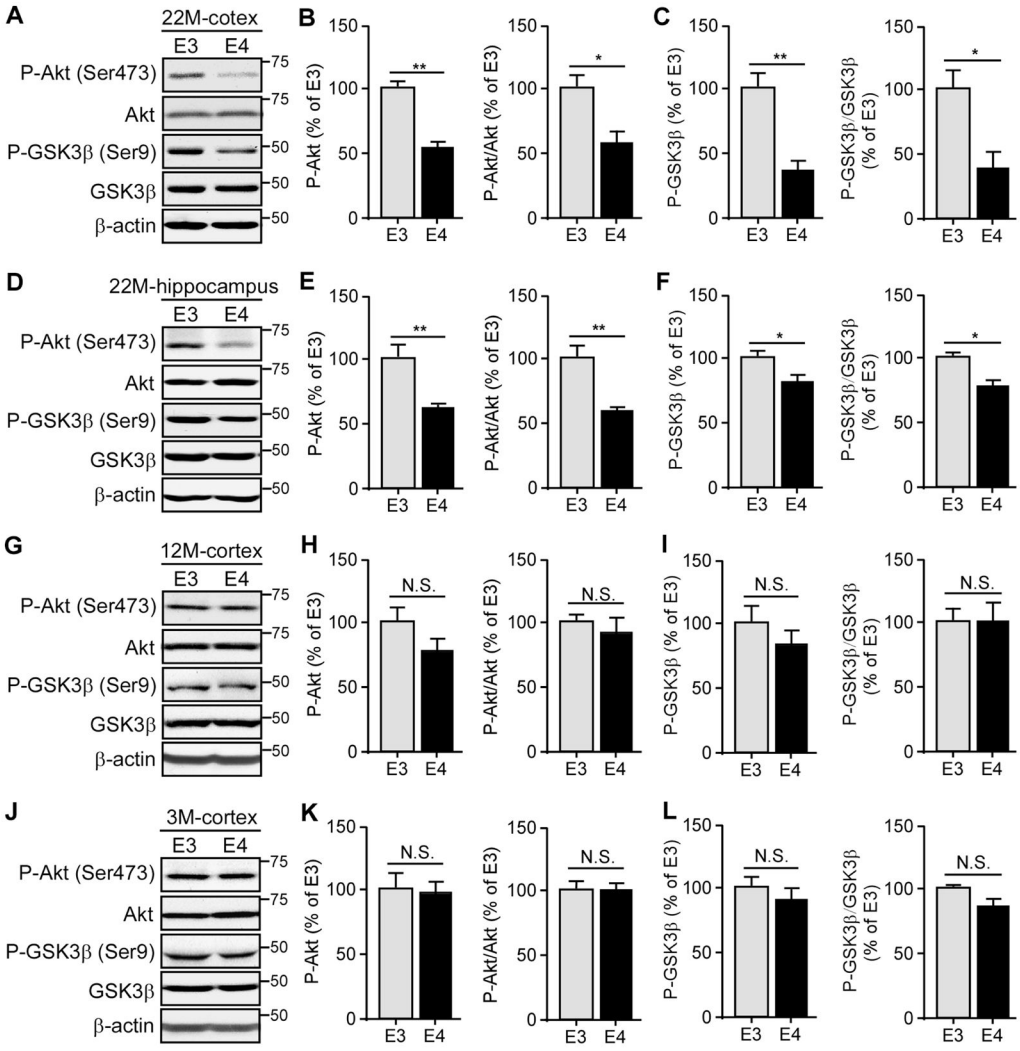


**Figure 1. ApoE4 Impairs Cerebral Basal Insulin Signaling in an Age-dependent Manner. See also Figure S1 and S2**

Brain lysates from apoE3-TR and apoE4-TR mice (n=4–6 mice/genotype, mixed gender) at 22 months (A–F), 12 months (G–I) and 3 months (J–L) of age were prepared and the amount of p-Akt (Ser473), total Akt, p-GSK3β (Ser9) and total GSK3β in the cortex (A–C, G–L) and hippocampus (D–F) was examined by Western blotting. Results were normalized to β-actin levels. The ratios of p-Akt/total Akt and p-GSK3β/total GSK3β were quantified and calculated. Data are expressed as mean ± SEM relative to apoE3-TR mice. Two-tailed student's *t* test was used for statistical analysis. *p < 0.05; **p < 0.01, N.S., not significant. Molecular mass markers in kilodaltons are shown.

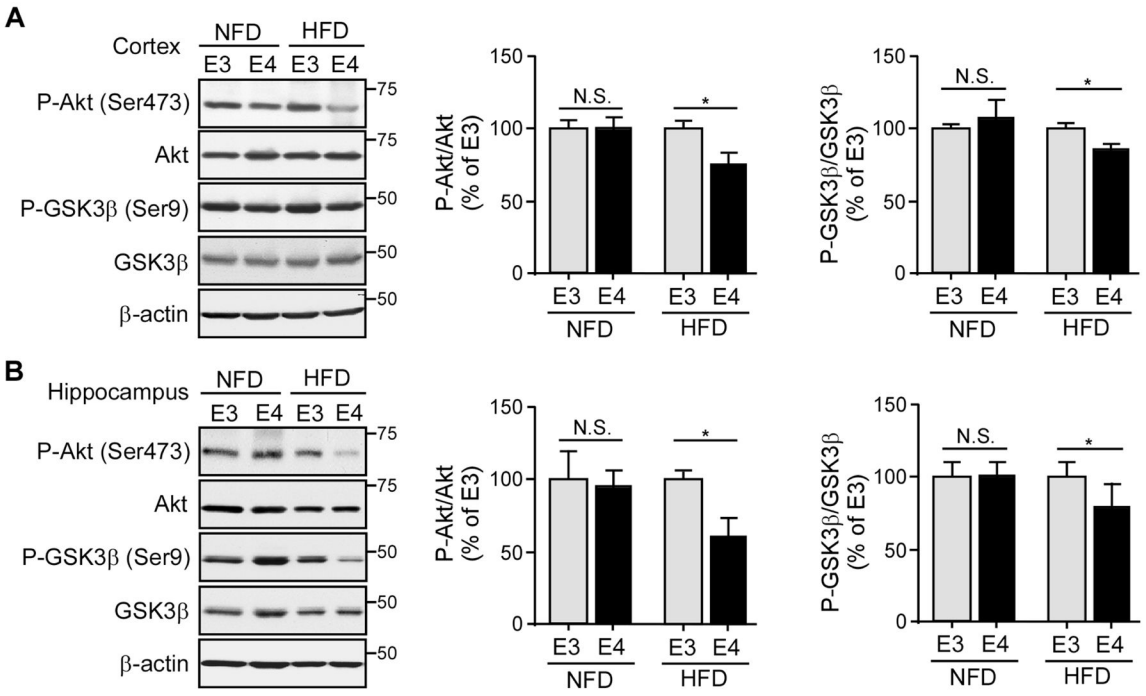


**Figure 2. HFD Treatment Accelerates the Age-dependent Impairment of Cerebral Basal Insulin Signaling in ApoE4-TR Mice**

ApoE3-TR and apoE4-TR mice (n=8–9 mice/genotype/treatment group, mixed gender) at middle age (8 months) were fed with either NFD or HFD for 4 months. The amount of p-Akt (Ser473), total Akt, p-GSK3β (Ser9) and total GSK3β in the cortex (A) or hippocampus (B) was examined by Western blotting. The ratios of p-Akt/total Akt and p-GSK3β/total GSK3β were calculated. Data were normalized to apoE3-TR mice for comparison. Two-tailed student's *t* test was used for statistical analysis within the group. *$p < 0.05$; N.S., not significant. Molecular mass markers in kilodaltons are shown.

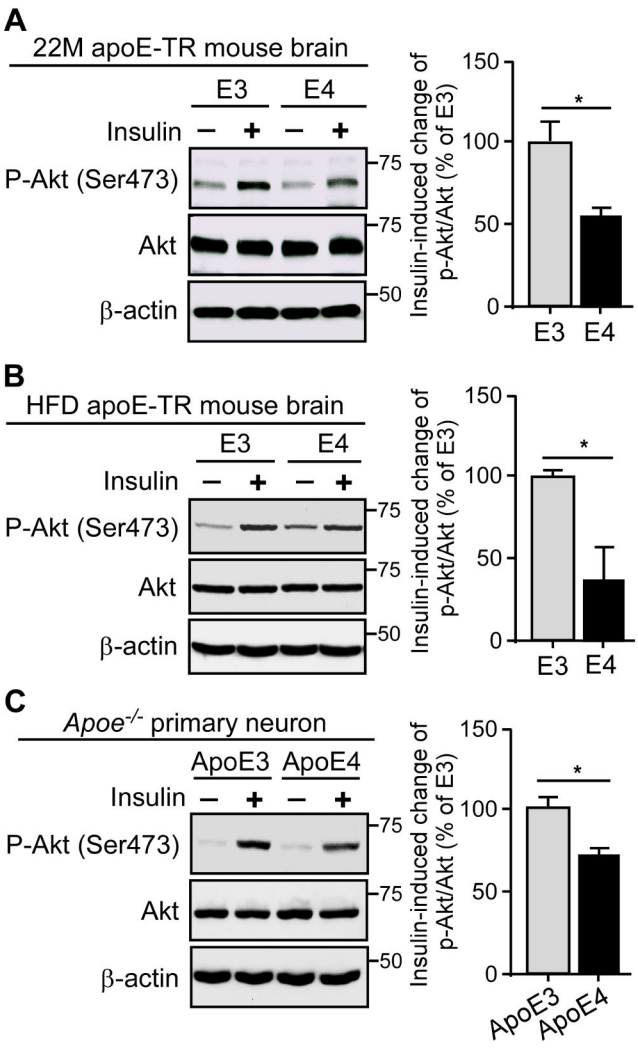


**Figure 3. ApoE4 Reduces Insulin-induced Sensitivity to Insulin Signaling. See also Figure S3**

(A and B) The amount of hippocampal p-Akt (Ser473), total Akt and β-actin in old (22 months) apoE-TR mice (A) or HFD-treated middle-age (12 months) apoE-TR mice (B) was examined by Western blotting after insulin treatment via reverse microdialysis (n=4 mice/genotype, male). Results were normalized to β-actin levels. Both contralateral (without insulin) and ipsilateral (with insulin) hippocampal homogenates from the same animal were analyzed on the same blot and the change in p-Akt/total Akt ratio in response to insulin treatment was calculated. Data were normalized to apoE3-TR mice for comparison. (C) *Apoe*$^{-/-}$ primary neurons were treated overnight with 50 nM recombinant apoE3 or apoE4 followed by insulin treatment (100 nM) for 30 minutes. The amount of p-Akt (Ser473), total Akt and β-actin was detected by Western blotting (three independent experiments). The change in p-Akt/total Akt ratio after insulin treatment was calculated. Data were normalized to apoE3 treatment for comparison. Values are expressed as mean ± SEM. Two-tailed student's *t* test was used for statistical analysis. *$p < 0.05$. Molecular mass markers in kilodaltons are shown.

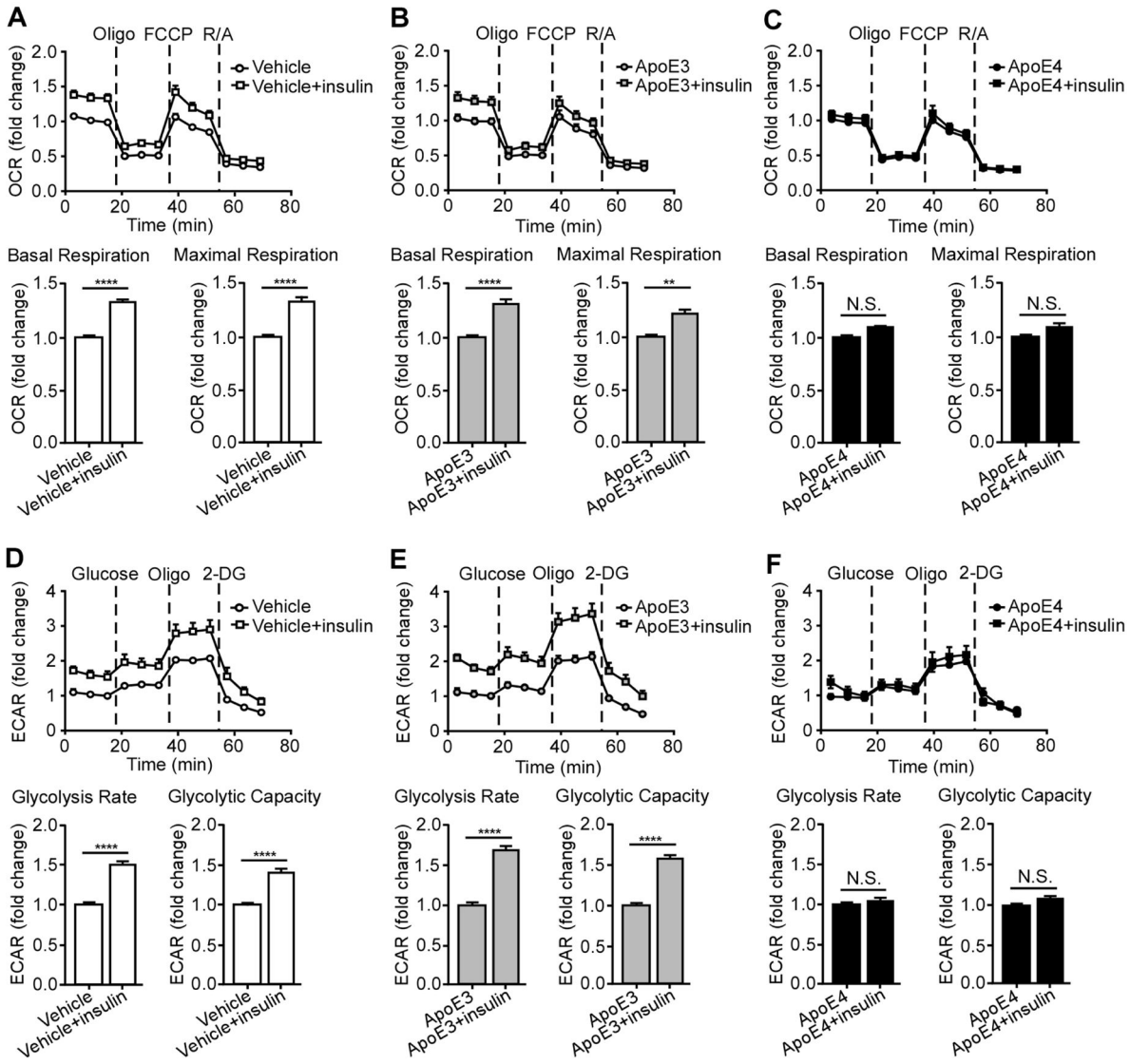


**Figure 4. ApoE4 Inhibits Insulin-induced Mitochondrial Respiration and Glycolysis. See also Figure S4**

Mitochondrial respiration and glycolysis were measured by Seahorse XFe96 analyzer in *Apoe*$^{-/-}$ neurons treated overnight with vehicle or 50 nM recombinant apoE3 or apoE4 followed by insulin (100 nM) treatment for 30 minutes. (A–C) Oxygen consumption rate (OCR) was assessed over time after sequential injections of 2 μM oligomycin, 1 μM FCCP, and 5 μM rotenone/antimycin A. The basal respiration and the maximal respiration were calculated to compare the effect of insulin treatment. (D–F) The extracellular acidification rate (ECAR) was assessed over time after sequential injections of glucose (10 mM), oligomycin (2 μM) and 2-DG (50 mM). The glycolysis rate and glycolytic capacity were calculated to compare the effect of insulin treatment. Each value was derived from 10 to 12 repeats in two independent experiments and normalized to the third data point measurement of baseline from non-insulin treatment group for comparisons. Data are expressed as mean ± SEM. Two-tailed student's *t* test was used for statistical analysis. ****$p < 0.0001$; N.S., not

significant. Oligo, Oligomycin; FCCP, Carbonyl cyanide-p-trifluoromethoxyphenylhydrazone; RA, rotenone/antimycin A.

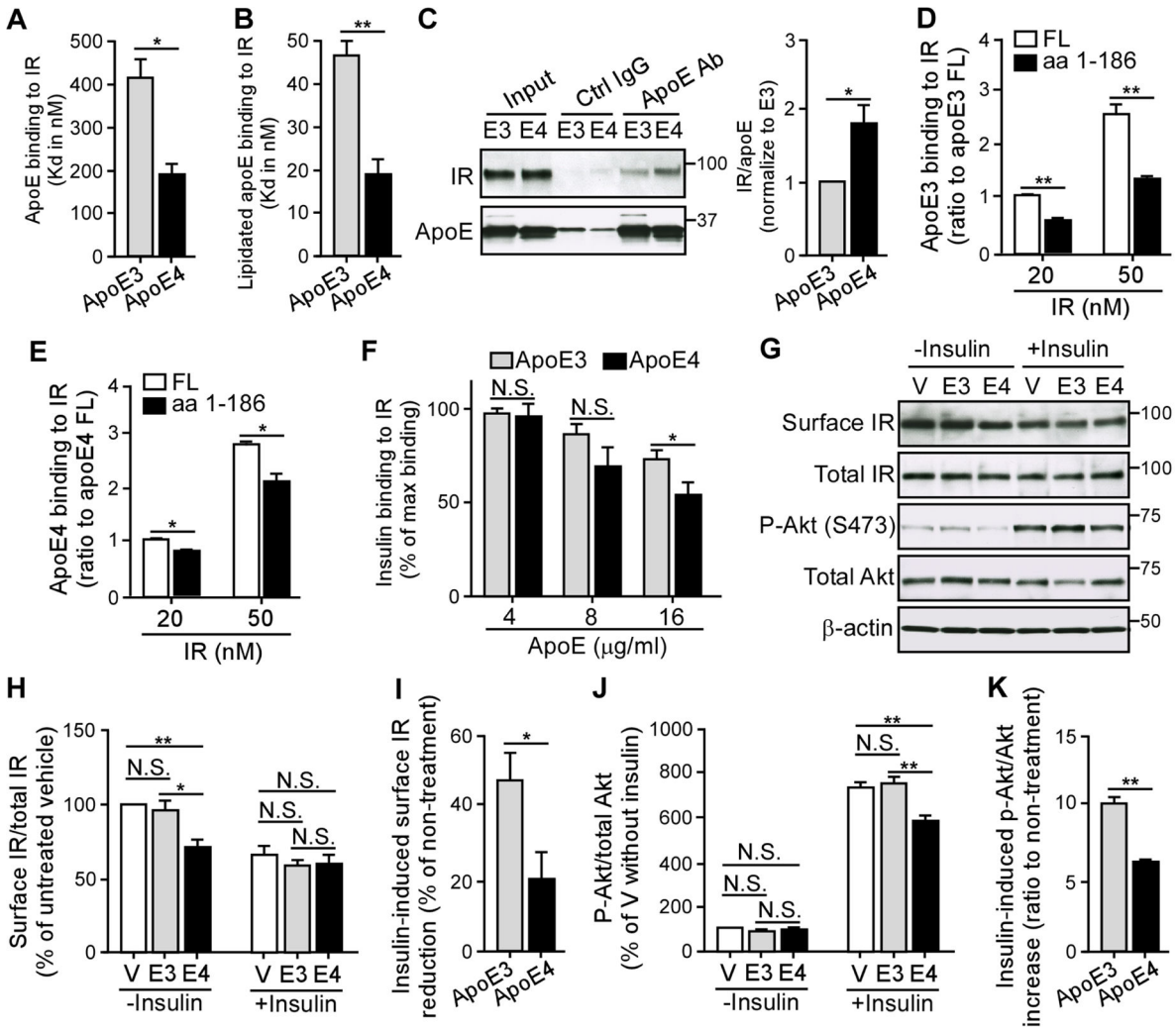


**Figure 5. ApoE4 Suppresses the Amount of Cell Surface IR. See also Figure S5–S9**

(A and B) The interaction between IR and recombinant apoE (A) or astrocyte-secreted lipidated apoE particles (B) were evaluated by solid-phase binding assay (three independent experiments). The Kd values of the binding curves were calculated using the one-site specific binding equation. (C) The interaction between IR and recombinant apoE was evaluated by solution binding assay, followed by immunoprecipitation (IP) of apoE and immunoblotting (IB) of IR. The ratio of IR to apoE was calculated. The values were normalized to apoE3 for comparison. (D–E) The domain interaction between apoE and IR was determined by solid-phase binding assay (three independent experiments) using C-terminal truncated apoE3 or apoE4 containing the aminol acid (aa) 1-186 compared with the full-length (FL) of apoE. The values were normalized to the binding of apoE FL for comparison. (F) A competitive inhibition assay of insulin (8 nM), IR (80 nM) and apoE (4, 8, or 16 μg/ml) was analyzed using solid-phase binding assay (three independent experiments). Results were normalized to the maximal binding of insulin and IR in the absence of apoE. (G–K) Primary *Apoe*$^{-/-}$ neurons were treated overnight with recombinant apoE3 or apoE4 (100 nM) in the presence or absence of insulin (100 nM) stimulation for 30

minutes, followed by cell surface biotinylation assay and Western blot analysis (three independent experiments). The cell surface IR and total IR were shown and the ratio of cell surface IR/total IR was calculated (G, H). The values were normalized to the vehicle-treated group (V) for comparison. The change in cell surface IR/total IR after insulin treatment was evaluated (I). The amount of p-Akt (Ser473), total Akt and β-actin was detected by Western blotting (G, J, K). Ratio of p-Akt to total Akt (J) and insulin-induced p-Akt/Akt change (K) were calculated. The values were normalized to vehicle without insulin treatment group for comparison. All data represent mean ± SEM. Two-tailed student's *t* test (A–C, F, I, K) and one-way ANOVA with Tukey's multiple comparisons test (D, E, H, J) were used in for statistical analysis. *$p < 0.05$; **$p < 0.01$; N.S., not significant. Molecular mass markers in kilodaltons are shown.

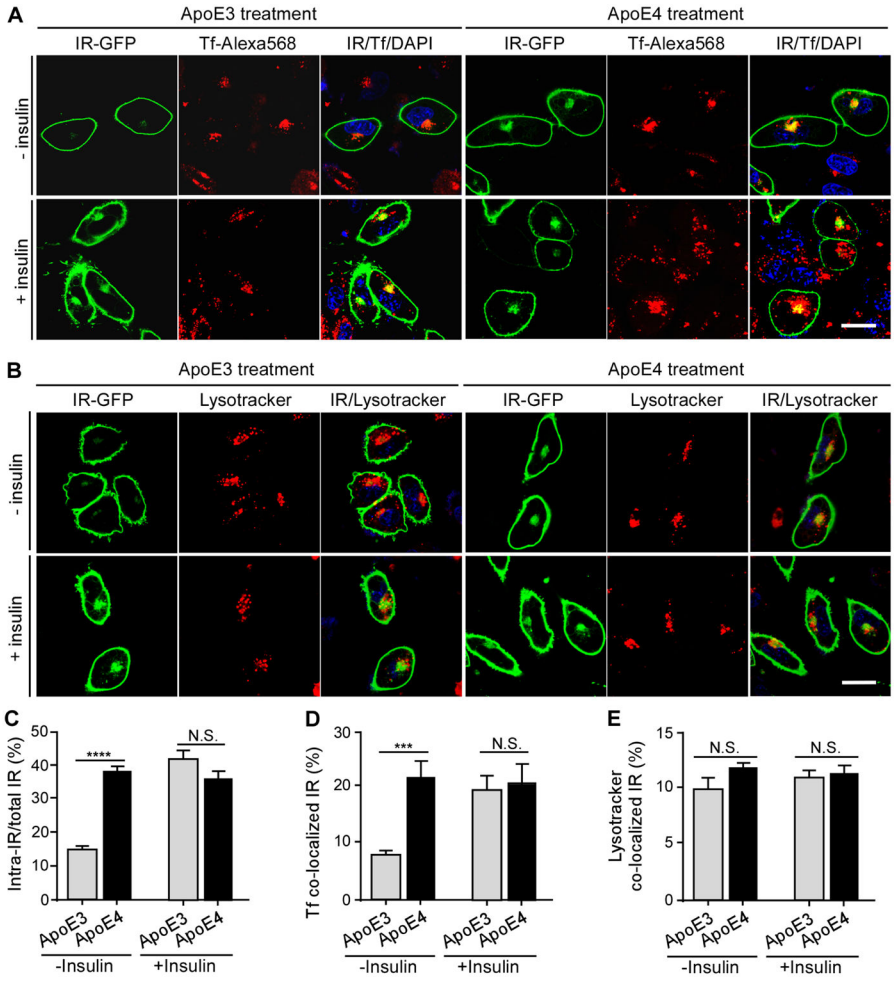


**Figure 6. ApoE4 Impairs IR Trafficking by Trapping IR in the Endosome. See also Figure S8 and S9**

SH-SY5Y neuronal cells transfected with human IR-GFP were treated overnight with recombinant apoE3 or apoE4 (100 nM) in the presence or absence insulin (100 nM) stimulation for 30 minutes. Alexa Flour 568-labeled human transferrin (Tf, 20 μg/ml) or Lysotracker (10 μM) was added to the medium one hour before fixing the cells and images were obtained by confocal microscopy. (A) The co-localization of IR-GFP (Green) and Tf (Red) in apoE3- and apoE4-treated cells in the presence and absence of insulin is shown. DAPI (blue) was included to position the nucleus. (B) The co-localization of IR-GFP (Green) and Lysotracker (Red) in apoE3- and apoE4-treated cells in the presence and absence of insulin is shown. DAPI (blue) was included to position the nucleus. (C) Percentage of intracellular IR (intra-IR/total IR) was calculated. (D) Percentage of IR that was co-localized with Tf (Tf co-localized IR) was calculated. (E) Percentage of IR that was co-localized with Lysotracker (Lysotracker co-localized IR) was calculated. Data from three independent experiments are expressed as mean ± SEM. Two-tailed student's *t* test was used for statistical analysis. ***p < 0.001; ****p < 0.0001; N.S., not significant. Scale bar, 20 μm.

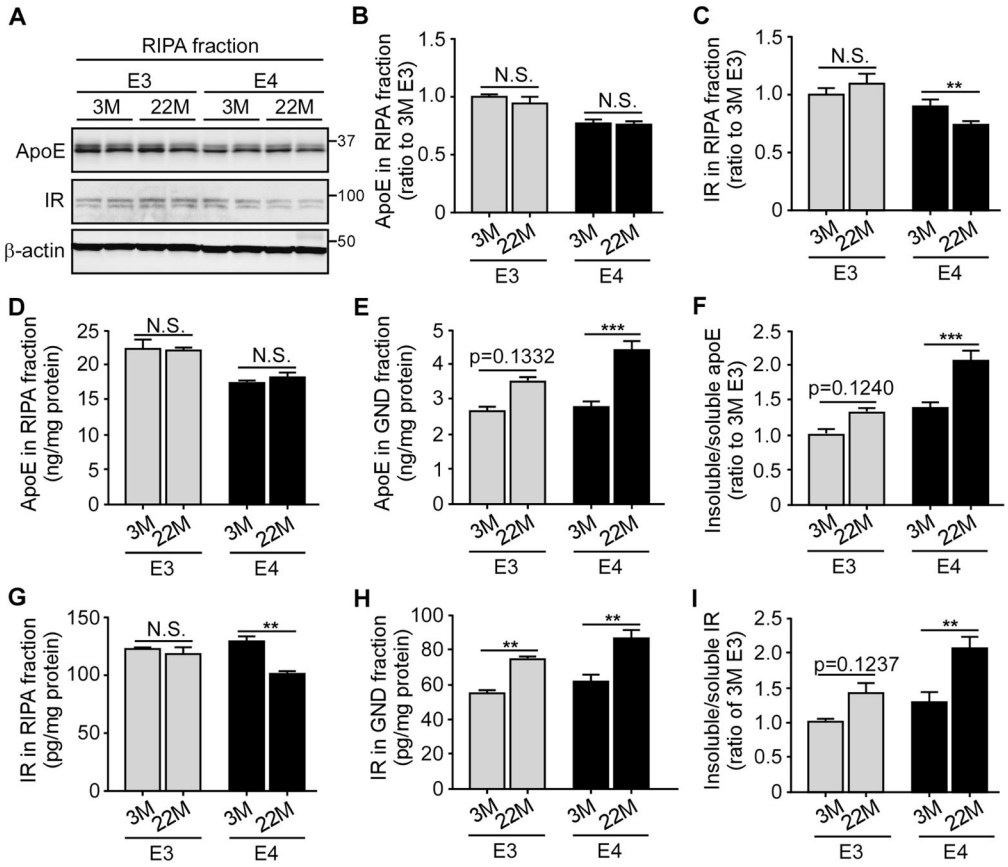


**Figure 7. ApoE4 Aggregation in Aging Brain Accelerates the Insolubility of IR**

RIPA and guanidine (GND)-extracted brain cortical lysates of apoE3-TR and apoE4-TR mice (n=4–6 mice/genotype, mixed gender) at 3 and 22 months of age were prepared and the amount of apoE and IR was examined by Western blotting (A–C) and ELISA (D–I). Results were normalized to β-actin levels in Western blot analysis. The ratios of insoluble (GND fraction) to soluble (RIPA fraction) apoE (F) and IR (I) were calculated. Data are expressed as mean ± SEM. Two-way ANOVA with Tukey's multiple comparisons test was used for statistical analysis. **p < 0.01; ***p < 0.001, N.S., not significant. Molecular mass markers in kilodaltons are shown.

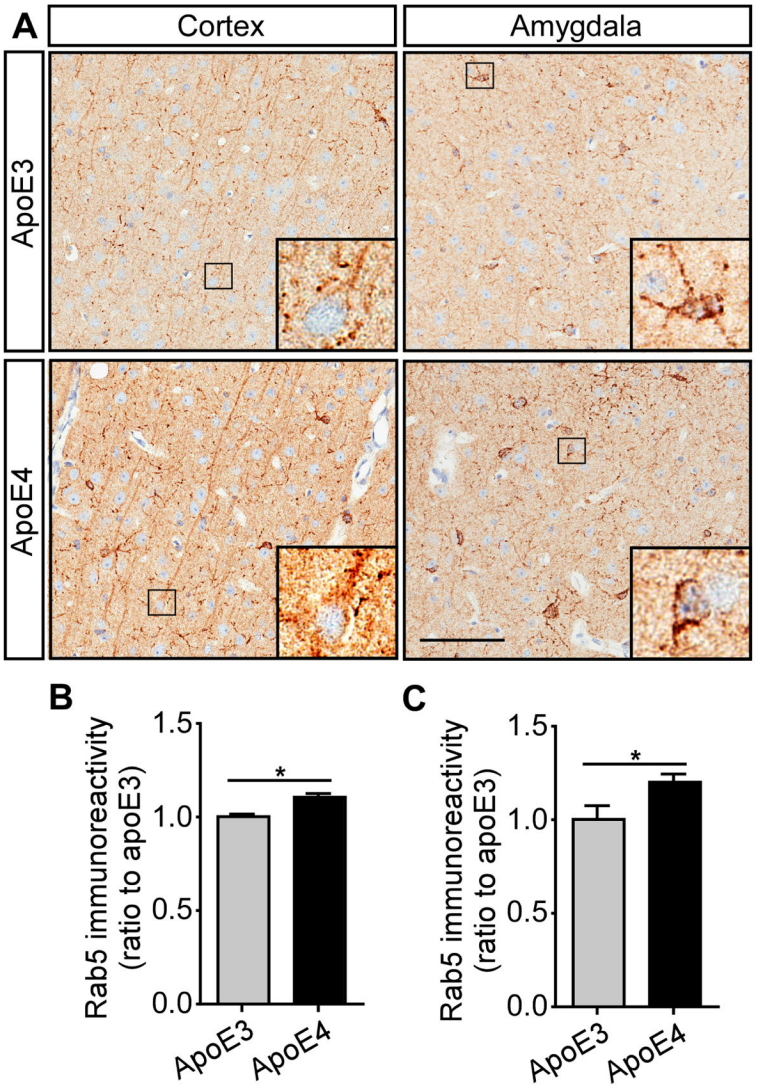


**Figure 8. Aged ApoE4-TR Mice Exhibit Elevated Early Endosomal Marker. See also Figure S10**

Brain slices from apoE3-TR and apoE4-TR mice at 22 months of age were prepared, and the early endosomes were examined by immunohistochemical staining for Rab5. The Rab5 expression pattern in the cortex and amygdala is shown (A). Scale bar, 100 μm. (B and C) The immunoreactivity of Rab5 staining in the cortex and amygdala from apoE3-TR and apoE4-TR mice was quantified using Aperio ImageScope (n=6 mice/genotype, mixed gender). Data are expressed as mean ± SEM relative to apoE3-TR mice. Two-tailed student's *t* test was used for statistical analysis. *p<0.05.